Baseline vector repeatability at the sub-millimeter level enabled by radio interferometer phase delays of intra-site baselines

Ming Hui Xu[1], Tuomas Savolainen[1], Sergei Bolotin[2], Simone Bernhart[3], Christian Plötz[4], Rüdiger Haas[5], Eskil Varenius[5], Guangli Wang[6], Jamie N McCallum[7], Robert Heinkelmann[8], Susanne Lunz[9], Harald Schuh[10], Nataliya Zubko[11], and Niko Kareinen[11]

[1]Aalto University
[2]NVI,Inc.
[3]Reichert GmbH / BKG
[4]Geodetic Observatory Wettzell, Federal Agency for Cartography and Geodesy
[5]Department of Space, Earth and Environment, Onsala Space Observatory, Chalmers University of Technology
[6]Shanghai Astronomical Observatory (CAS)
[7]University of Tasmania
[8]GFZ Potsdam
[9]GFZ German Research Centre for Geosciences
[10]GFZ
[11]Finnish Geospatial Research Institute

November 25, 2022

Abstract

We report the results of position ties for short baselines at eight geodetic sites based on phase delays that are extracted from global geodetic very-long-baseline interferometry (VLBI) observations rather than dedicated short-baseline experiments. An analysis of phase delay observables from two antennas at the Geodetic Observatory Wettzell, Germany, extracted from 107 global 24-hour VLBI sessions since 2019 yields weighted root-mean-square scatters about the mean baseline vector of 0.3, 0.3, and 0.8 mm in the east, north, and up directions, respectively. Position ties are also obtained for other short baselines between legacy antennas and nearby, newly built antennas. They are critical for maintaining a consistent continuation of the realization of the terrestrial reference frame, especially when including the new VGOS network. The phase delays of the baseline WETTZ13N–WETTZELL enable an investigation of sources of error at the sub-millimeter level. We found that a systematic variation of larger than 1 mm can be introduced to the up estimates of this baseline vector when atmospheric delays were estimated. Although the sub-millimeter repeatability has been achieved for the baseline vector WETTZ13N–WETTZELL, we conclude that long term monitoring should be conducted for more short baselines to assess the instrumental effects, in particular the systematic differences between phase delays and group delays, and to find common solutions for reducing them. This will be an important step towards the goal of global geodesy at the 1 mm level.

Baseline vector repeatability at the sub-millimeter level enabled by radio interferometer phase delays of intra-site baselines

Ming H. Xu[1,2,10], Tuomas Savolainen[1,2], Sergei Bolotin[3], Simone Bernhart[4], Christian Plötz[5], Rüdiger Haas[6], Eskil Varenius[6], Guangli Wang[7], Jamie McCallum[8], Robert Heinkelmann[9], Susanne Lunz[10], Harald Schuh[10,9], Nataliya Zubko[11], and Niko Kareinen[11]

[1]Aalto University Metsähovi Radio Observatory, Metsähovintie 114,02540 Kylmälä, Finland
[2]Aalto University Department of Electronics and Nanoengineering, PL15500, FI-00076 Aalto, Finland
[3]NVI Inc. at NASA Goddard Space Flight Center, Code 61A.0, Greenbelt, MD, 20771, USA
[4]Reichert GmbH/Bundesamt für Kartographie und Geodäsie, 53121 Bonn, Germany
[5]Geodetic Observatory Wettzell, Federal Agency for Cartography and Geodesy, Sackenrieder Str. 25, 93444 Bad Kötzting, Germany
[6]Department of Space, Earth and Environment, Onsala Space Observatory, Chalmers University of Technology, 439 92 Onsala, Sweden
[7]Shanghai Astronomical Observatory, Chinese Academy of Sciences, No. 80 Nandan Raod, 200030, Shanghai, P. R. China
[8]School of Natural Sciences, University of Tasmania, Private Bag 37, Hobart TAS 7001, Australia
[9]DeutschesGeoForschungsZentrum (GFZ), Potsdam, Telegrafenberg, A17, 14473 Potsdam, Germany
[10]Institute of Geodesy and Geoinformation Science, Technische Universität Berlin, Straße des 17. Juni 135, 10623, Berlin, Germany
[11]Finnish Geospatial Research Institute, Geodeetinrinne 2, FIN-02430 Masala, Finland

Key Points:

- Baseline vectors of legacy antennas and co-located, new antennas are obtained from phase delays with the highest possible accuracy.
- Sources of error in short-baseline observations are investigated at the 1 mm level.

Corresponding author: Ming H. Xu, `minghui.xu@aalto.fi`

Abstract

We report the results of position ties for short baselines at eight geodetic sites based on phase delays that are extracted from global geodetic very-long-baseline interferometry (VLBI) observations rather than dedicated short-baseline experiments. An analysis of phase delay observables from two antennas at the Geodetic Observatory Wettzell, Germany, extracted from 107 global 24-hour VLBI sessions since 2019 yields weighted root-mean-square scatters about the mean baseline vector of 0.3, 0.3, and 0.8 mm in the east, north, and up directions, respectively. Position ties are also obtained for other short baselines between legacy antennas and nearby, newly built antennas. They are critical for maintaining a consistent continuation of the realization of the terrestrial reference frame, especially when including the new VGOS network. The phase delays of the baseline `WETTZ13N–WETTZELL` enable an investigation of sources of error at the sub-millimeter level. We found that a systematic variation of larger than 1 mm can be introduced to the up estimates of this baseline vector when atmospheric delays were estimated. Although the sub-millimeter repeatability has been achieved for the baseline vector `WETTZ13N–WETTZELL`, we conclude that long term monitoring should be conducted for more short baselines to assess the instrumental effects, in particular the systematic differences between phase delays and group delays, and to find common solutions for reducing them. This will be an important step towards the goal of global geodesy at the 1 mm level.

Plain Language Summary

We report the results of position ties for short baselines at eight geodetic sites based on phase delays that are extracted from global geodetic very-long-baseline interferometry (VLBI) observations rather than dedicated short-baseline experiments. By using the inherently more precise observables - phase delays, a baseline vector repeatability of `WETTZ13N–WETTZELL` has been achieved at the sub-millimeter level for the horizontal directions and at the 1 millimeter (mm) level for the vertical direction based on VLBI experiments of 107 days during 3.5 years. Position ties based on phase delays are also obtained for other short baselines between legacy antennas and nearby, newly built antennas, and they are critical to maintain a consistent continuation of the realization of terrestrial reference frame into the future of a network of these new antennas. We have evaluated the instrumental stability at the 1 mm level, which is an important step towards the goal of global geodesy at this level.

1 Introduction

The technique of very-long-baseline interferometry (VLBI) combines the signal of a radio source recorded by a pair of radio antennas to provide the delay, both phase delay and group delay, of the arrival times at the two antennas. It was initially developed for astronomy in the late 1960s to derive high angular resolution images for celestial objects and was later also used for geodesy to determine the orientation of the Earth in space and the positions of the antennas on the Earth with a high precision (see, Sovers et al., 1998, and the references therein). In astronomy, the highest accuracy is obtained by making use of the full precision of phase delays for relative measurements between pairs of nearby objects on the sky. Phase delays can be also used in geodesy to obtain relative positions between nearby antennas on the Earth with the highest accuracy.

In the transition period of the geodetic VLBI systems, phase delays of short baselines enable significant scientific applications. Many antennas of the legacy VLBI system which is mainly based on dual-band observations (2.3 Ghz and 8.4 GHz), though being continuously upgraded and still used, have reached the limits of their capability; this legacy system is pushed to the limits also because the Earth science studies continue to pursue more precise geodetic measurements. The next-generation geodetic VLBI system, known as the VLBI Global Observing System (VGOS; Niell et al., 2007; Petrachenko et al., 2009), has been developing worldwide with antennas of relatively small diameter, 12–13 m, and broadband receivers, 2.0 − 14.0 GHz, with the aim to achieve 1 mm station position accuracy and 0.1 mm/yr velocity stability on global scales. It is necessary to accurately tie these new, small antennas to the legacy, co-located antennas that have a long observing history since 1979 and have been playing a fundamental role in the realizations of the International Terrestrial Reference Frame (ITRF; Altamimi et al., 2016) to allow for a consistent continuation of the ITRF into the VGOS era. Recently, dedicated position tie measurements of this type have been performed, for instance, for the legacy antenna and the VGOS antenna at the Kokee Park Geophysical Observatory by Niell et al. (2021) and for the legacy antenna and the twin VGOS antennas at the Onsala Space Observatory by Varenius et al. (2021). An alternative way to derive these position ties is to make use of the global geodetic VLBI observations by the International VLBI Service for Geodesy and Astrometry (IVS; Schuh & Behrend, 2012; Nothnagel et al., 2017, see `https://ivscc.gsfc.nasa.gov/index.html`).

In this work, we analyze the observed phase delays to obtain position ties for as many co-located legacy and VGOS-compatible antennas and as many observations as possible. Our purpose is twofold: (1) to determine the baseline vectors between the legacy antennas and the co-located, new antennas with the highest possible accuracy and (2) to investigate the baseline vector repeatability of the short baselines determined from a time series of VLBI observations. The latter will allow us to separate the purely instrumental effects, affecting both short-baseline and long-baseline observables and dominating the estimates of the short-baseline vectors, from other contributions due to geophysical/astrophysical effects. The goal of this study is to contribute to the effort of the consistent continuation of the global Terrestrial Reference Frame (TRF) and to investigate the sources of error, mainly the instrumental effects, in VLBI observations.

2 Data and data analysis

We analyzed the IVS observations to derive the position ties for the antennas shown in Fig. 1. The routine geodetic solutions of these global sessions have already been submitted by IVS analysis centers to the IVS combination center, which combines the results and provides the VLBI inputs for building the ITRF. (For the latest ITRF2020, the IVS analysis activities can be found at `https://ivscc.gsfc.nasa.gov/IVS_AC/IVS-AC_ITRF2020.htm`.) However, the short-baseline observables in these global geodetic VLBI observations can be analyzed independently from the observations of the entire network in each session in order to obtain the baseline vectors with the highest accuracy. The reasons are as follows:

1. In the routine geodetic VLBI solutions, observables at both S and X band are required to remove the dispersion affecting the radio signal when it passes through the charged medium, mainly the ionosphere. Any local radio interference, which is highly correlated for antennas at the same site, contributes large noise to the S band observables and thus to the ionospheric-free observables, though scaled down by a factor of 13.8. More importantly, false detections at S band lead to flagging the corresponding observables at X band as bad, and in not uncommon cases the observations of an antenna in one session are completely lost in the final data analysis due to the issues that happened only at S band. (See the comparison for baseline `NYALES13S`–`NYALES20` in Sect. 3.1.2.) However, the observables at S band are not needed for short baselines, as the ionospheric effect is negligible for co-located antennas (pointing to a common source).

2. The position estimates of the co-located antennas treated independently in a geodetic solution of a full session are affected by systematic error sources, such as source structure, ionosphere, and atmosphere. In contrast, these systematic errors impose minimum impacts on the short-baseline observables.
3. Thermal noise can be one of the dominant errors in the short-baseline group delay observables, and it is significantly reduced by using phase delay observables (Ray & Corey, 1991).
4. Some of these short baselines are regularly scheduled in the VLBI sessions having a duration of one hour for the rapid determination of the highly variable Earth's rotation, called Intensive sessions, which by their design are not intended to be used for deriving station positions. They allow us to investigate the position accuracy that can be obtained from short-time observations, like the Intensive sessions.

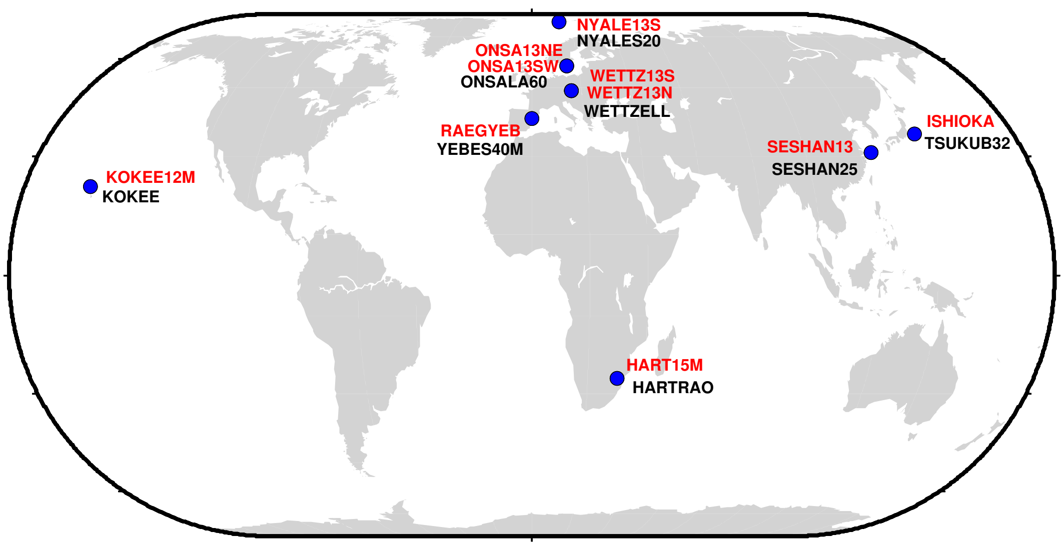

Figure 1. Radio telescopes with position tie measurements reported in this study. At each VLBI site (blue dot), there is a legacy telescope (black designator) and at least one new telescope (red designator).

2.1 Observations

In addition to the dedicated experiments for the Onsala antennas (the ONTIE sessions) that were reported in Varenius et al. (2021) and the Kokee antennas reported in Niell et al. (2021), short-baseline observations were found in three types of geodetic sessions: regular 24-hour sessions, special sessions of a combined network from legacy antennas and VGOS antennas, and Intensive sessions. The total number of the VLBI sessions (of these three types) analyzed in this study and the baseline lengths are reported in Table 1. Baseline `ONSA13NE–ONSA13SW` is formed by two VGOS antennas; each of the other ten baselines consists of a legacy antenna and a new antenna with a small diameter in the 12–15 m range. The broadband receivers used in the VGOS system record the linearly polarized components of a signal, denoted by H and V, whereas the receivers of the legacy antennas are designed to record right-hand circular polarization, denoted by R. In the current data processing of VGOS observations, the pseudo-Stokes I visibilities are formed from the four linear polarization correlation products due to lack of knowledge of the crosspolarization "D" terms (see https://www.haystack.mit.edu/wp-content/uploads/2020/07/docs_hops_000_vgos-data-processing.pdf). For a mixed baseline of a legacy antenna and a VGOS antenna, a combined product of $RH{+}RV$ is formed; the observations including these baselines in the network are referred to as the mixed-mode sessions. For the observations analyzed in this work, the first five baselines of Table 1 were observed in legacy S/X mode, and the remaining six baselines were observed in mixed mode. The new antennas involved in the first five baselines may have observed with a broadband receiver in other sessions or may be upgraded as a VGOS antenna in the future.

Table 1. Short baselines analyzed in the study, the numbers of sessions, and the baseline lengths.

Baseline	2-letter code[1]	Number of sessions	Length (m)
WETTZ13N–WETTZELL	Wn-Wz	165[2]	123
NYALE13S–NYALES20	Ns-Ny	19	1539
ISHIOKA–TSUKUB32	Is-Ts	17	16606
HARTRAO–HART15M	Hh-Ht	8	113
SESHAN13–SESHAN25	S6-Sh	1	56
WETTZ13S–WETTZELL	Ws-Wz	2	187
RAEGYEB–YEBES40M	Yj-Ys	1	194
KOKEE12M–KOKEE	K2-Kk	1	31
ONSALA60–ONSA13SW	On-Ow	2	540
ONSA13NE–ONSALA60	Oe-On	1	469
ONSA13NE–ONSA13SW	Oe-Ow	1	75

[1]The 2-letter codes of geodetic VLBI antennas are available from https://cddis.nasa.gov/archive/vlbi/ivscontrol/ns-codes.txt. [2]These consist of 107 global 24-hour sessions and 58 Intensives. The complete VLBI session list per year is available from https://ivscc.gsfc.nasa.gov/program/master.html.

2.2 Phase ambiguity

For geodetic VLBI observations in the legacy mode and the mixed mode, a multi-dimensional Fourier search from fringe phases of an interferometer gives (multi-band) group delay, delay rate, and visibility phase. The group delay is the derivative of phase with respect to frequency, whereas the phase delay is obtained as the ratio of the visibility phase to frequency. Phase delays intrinsically have higher precision than group delays, however, they are typically not used in routine geodetic solutions due to unknown phase turns, i.e. phase ambiguities.

Phase delay differs from group delay in terms of (1) the instrumental effects, such as the rotation of the feeds, the dispersion of the signal in the antenna system itself, and the signal delays in the waveguides prior to the injection of the phase calibration signals, (2) the frequency-dependent astronomical effects, the dispersive nature of the plasma along the line of sight and extended structure of radio sources, and (3) the magnitude of the thermal noise. The instrumental effects, which can be very large, either can be calibrated or are expected to be constant. The integrated plasma densities along the line of sight have very small differences for the co-located antennas of a short baseline. Most of the radio sources in the geodetic catalog, after a refinement over 40 years, are compact at the arcsecond scale, and the effects of structure for the majority of the sources at the scale of milli-arcsecond are relatively small for the short-baseline observations (see, e.g., Xu et al., 2016, 2019). For short baselines, the uncertainties of group delays due to thermal noise are generally far smaller than the phase ambiguity spacing. In the cases where the group delays are very noisy, for instance on the baseline `NYALE13S`–`NYALES20`, theoretical delays instead of the group delay observables can be used for directly aligning the phases over time, assuming that the unpredictable effects on the short baselines change relatively smoothly. Exceptional cases can happen when antennas have very unstable clocks or the a priori station position is very poorly known. The third option is to do a geodetic solution based on group delay observables for estimating the clock parameters and the station positions and then to employ them to connect the phases for resolving phase ambiguities.

The delay spacing of the phase ambiguities is about 120 ps at X band and about 450 ps at S band. In general, the variation of the differences between phase delays and group delays are expected to be relatively small compared to the ambiguity spacing, so that it is straightforward for most of the sessions to connect the phases over time. Yet there can still be (ambiguous) constant offsets between phase delays and group delays, which will be fully absorbed by the estimated clock offsets. (We should note that resolving phase ambiguity is generally challenging for long baselines because of the impacts of, for instance, atmosphere.) In this study about short baselines, we used the group delays to eliminate the 2π phase ambiguity of the corresponding phase delays and afterward examined the differences between the group delays and the phase delays for all observations of a baseline in a session. If the differences over time follow the pattern of a smooth curve with a scatter significantly smaller than half the ambiguity spacing, it is an indication of successful elimination of phase ambiguities, while a failure would be obvious through a random distribution of the differences within the ambiguity spacing. This method was used as an initial inspection. The other methods were used as alternatives for some of the baselines.

When phase calibration signals are too weak to be useful (or not available) for removing the instrumental phase variations between various frequency channels, the observations of radio sources with high flux densities can be used as an alternative to calibrate the instrumental phases, which makes the fringe fitting of group delays possible. This process is referred to as manual phase calibration. However, in this case one may not be able to connect the phases because of the variations of instrumental phases over time. The details of the correlation process are written in the IVS correlator reports. The feed rotation angle (FRA) corrections need to be considered even for these very short baselines, since the two antennas at one site can have different mounting types leading to differences in the FRA corrections, as is the case for the two antennas `HARTRAO` and `HART15M` (equatorial/altazimuth).

2.3 Comparison of group delays and phase delays

The differences between phase delays and group delays can be investigated after resolving phase ambiguities. These differences are shown in Fig. 2 for four cases as examples, which demonstrate that phase ambiguities can be reliably resolved based on group delay observables.

There can be systematic variations in the differences, which can change as much as 100 ps over an hour, as shown for baseline `WETTZ13N`–`WETTZELL` in session 21MAY10XA. When estimating only a constant clock offset and a clock rate over the 24 hours (two parameters), the delay residuals from a solution of group delays in the session have a similar pattern as the differences between group delays and phase delays, whereas the delay residuals based on phase delays are much smaller and flat. The delay residuals are shown in Fig. S1 of the supporting information. This result strongly suggests that the differences are introduced by the group delays. They are largely absorbed by the clock parameters in a full geodetic solution. These effects may be caused by the dispersion effects in the waveguides of the receivers prior to the injection of phase calibration signals, the undesired wave reflections within the antennas, and spurious phase calibration signals (see, e.g., Rogers, 1991). Note that instrumental instabilities of this size will cause difficulties for resolving phase ambiguities of the observations on long baselines including one of these two antennas. This is one of the obstacles when resolving phase ambiguities for global geodetic VLBI observations and will be discussed in a future study. Such large variability occurs in other sessions including this baseline and in observations of other short baselines as well. The systematic variations, though much smaller, are also visible on baseline `HARTRAO–HART15M` in South Africa and baseline `ISHIOKA–TSUKUB32` in Japan. Recovering phase ambiguities for an Intensive session is shown in the bottom panel of Fig. 2.

Based on closure analysis (see, e.g., Xu et al., 2016; Anderson & Xu, 2018; Xu et al., 2021), the inherently higher precision of phase delays can be seen directly at the observable level without a geodetic solution. Figure 3 shows the closure phase delays and closure group delays of triangle `ONSA13NE–ONSA13SW–ONSALA60` in session ON0080 (March 20, 2020). In principle, closures are sensitive only to the thermal noise and the effects of source structure, although the latter imposes minimum impacts on the observations of this small triangle for most of the geodetic sources. The unweighted and the weighted root-mean-square (rms) are 21.1 ps and 13.2 ps for the closure group delays, respectively, and they are 7.5 ps and 6.8 ps for the closure phase delays. Given that the thermal noise is independent among the three baselines, the noise level is about 12 ps in the group delays and 4 ps in the phase delays. Considering that the dominating source of error in the short-baseline observables is the thermal noise, this improvement in the accuracy of observables can lead to significantly better results.

2.4 Ionospheric corrections

The assumption that the ionospheric effect on short baseline is negligible can be validated after resolving phase ambiguities for both S band and X band observables. For baseline `WETTZ13N–WETTZELL` in session 21MAY10XA (a session with typical ionospheric delay corrections), the rms scatter of the ionospheric corrections at X band about the mean value, derived from the combination of the phase delays at S and X band, is less than 1 ps, and the peak-to-peak fluctuation is 3 ps. For baseline `NYALE13S–NYALES20`, about 1.5 km apart, the rms scatter is 2 ps with the peak fluctuation of 10 ps in session 21JUN24XE. For baseline `ISHIOKA–TSUKUB32`, about 16.6 km apart, the rms scatter and the fluctuation in session 16DEC20XA are similar to the values for the baseline `NYALE13S–NYALES20`.

In order to assess how much the S band observables corrupt the short-baseline observables in routine geodetic solutions, the rms scatters of the ionospheric corrections at X band, derived from the group delays at S and X band in the conventional way and restored in the databases, are calculated for the short baselines in the mixed mode session RD2005. The rms scatter is 15 ps with the peak fluctuation of about 100 ps for baseline `WETTZ13S–WETTZELL` of 0.2 km length and is 90 ps with the peak fluctuation of about 600 ps for baseline `ONSALA60–ONSA13SW` of 0.5 km length. As a direct comparison, the rms scatter of the ionospheric corrections in the IVS database of session 21JUN24XE for baseline `NYALE13S–NYALES20` is 120 ps. However, this is about two orders of magnitude larger than the real contribution of the ionospheric effects, as determined above by using the phase delays at the two bands. With this justification, the phase delays at S band were not used in our solutions because they can lead to flagging as outliers a significant amount of usable X band phase delays.

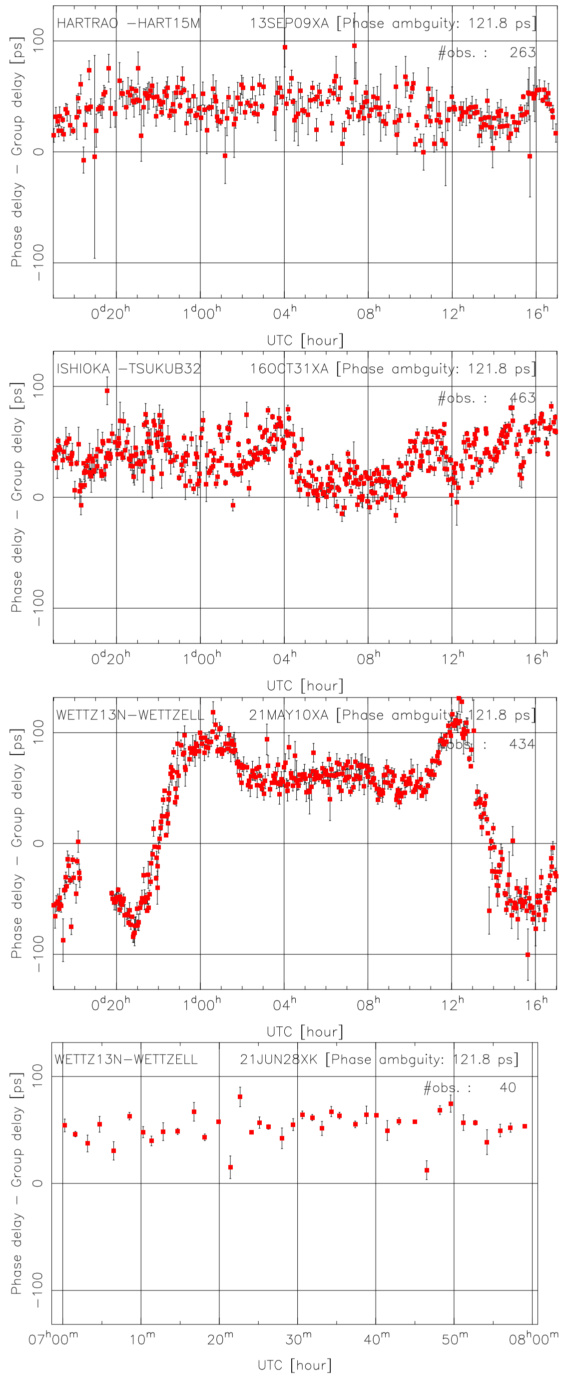

Figure 2. Demonstration of the differences between group delays and phase delays for baselines `HARTRAO–HART15M` (top), `ISHIOKA–TSUKUB32` (middle top), and `WETTZ13N–WETTZELL` (middle bottom) in 24-hour sessions and for baseline `WETTZ13N–WETTZELL` in a 1-hour session (bottom). Error bars shown are the combined uncertainties of the phase delays and the group delays. The plotting scale corresponds to about minus and plus one turn of phase.

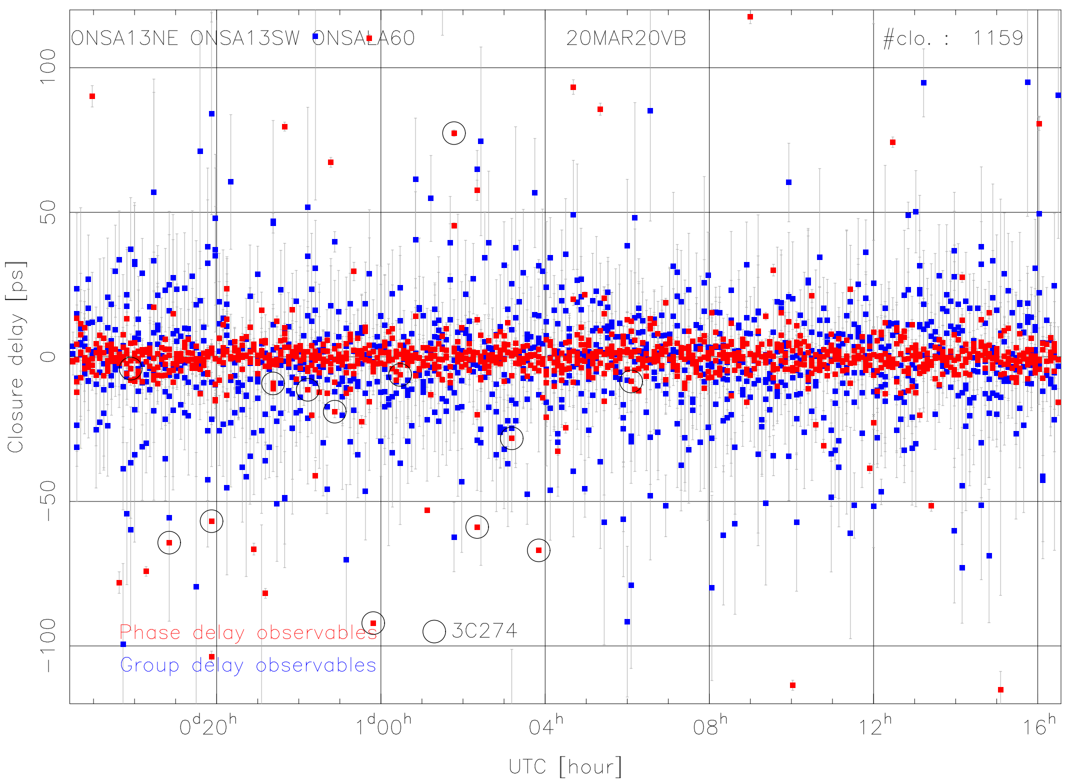

Figure 3. Comparison of closure group delays (blue squares) and closure phase delays (red squares) for the triangle `ONSA13NE`–`ONSA13SW`–`ONSALA60` in session ON0080 demonstrates the significantly higher precision of the phase delays than the group delays. The scatter of the closures indicates the contributions of thermal noise. The red squares marked by black circles indicate the observations of source 3C274, which is well known to have large scale structure and has a similar pattern in its closure phases from the other ONTIE sessions with these three antennas. The closures suggest that about 2% of the short-baseline observations may be significantly affected by source structure at large angular scales.

2.5 Data analysis

In the multiple steps of VLBI data processing (see https://ivscc.gsfc.nasa.gov/about/resolutions/IVS-Res-2019-02-AnalysisLevels.pdf), geodetic analysis is performed with the aim of estimating the parameters of geodetic interests, such as Earth orientation parameters (EOP), station positions, and source positions. In the geodetic solutions of short-baseline observations, there are two other possible kinds of parameters in addition to baseline vectors: clocks, accounting for the relative behaviors of the two frequency standards and for the instrumental delays, and differential zenith wet delays (dZWDs), accounting for the different atmospheric effects between the two antennas. The clocks were characterized by a continuous piece-wise linear (PWL) function with a time interval of usually one hour (but see the supporting information for additional discussion). For the atmospheric delays, the hydrostatic part was modeled, while the impact of the wet path delays due to water vapour was investigated by comparing the results of the baseline vector estimates from not estimating dZWDs and estimating them using PWL functions of different time intervals. Geodetic analysis was carried out by using either phase delays or group delays.

The software package *νSolve* (open source, available at https://sourceforge.net/projects/nusolve/) was used for the geodetic analyses. For each session, we reset the configuration in the original databases to remove the flagging and weighting information and the ionospheric corrections, excluded the observations of all antennas apart from the two antennas of the desired short baseline in a session, restored all the usable observables, examined and adjusted the phase ambiguities in a program developed by ourselves, flagged the outliers, and performed the solution based on either group delays or phase delays at X band. In geodetic solutions as guided by the *νSolve* user manual, one step that is commonly used is to determine a baseline-dependent uncertainty in addition to the formal error of each observable in order to derive a more realistic error used for the weighting; this additive uncertainty σ_{add} is a constant value in a session for each baseline and is determined in an iterative way until the reduced χ^2 is unity.

3 Results

When there are more than three sessions available for a baseline, the baseline vector repeatability is defined as the weighted root-mean-square (WRMS) scatter of the relative position estimates from these multiple sessions about the weighted mean value. We evaluated this metric for the three components of a baseline vector and present the results always in the sequence of the east, north, and up directions.

3.1 Baselines with more than two global sessions

3.1.1 WETTZ13N–WETTZELL

Geodetic/astrometric VLBI makes routine observations of tens of radio sources typically for 24 hours or for one hour in one session. These two antennas have simultaneously participated in these two types of IVS observations since 2015 (Schüler et al., 2015).

The correlator centers for processing VLBI observations by using the fringe fitting program *fourfit* started to apply a special mask called *notch* filter to mitigate the corruption due to specific phase calibration signals after October 2018. The width of such a notch filter depends on the spectral resolution which is used for correlation: the higher the resolution, the narrower the notch filters. Therefore, only the sessions since R4889 (April 11, 2019) or processed by the correlators after May 01, 2019 have usable observables on baseline `WETTZ13N–WETTZELL`. There are 107 sessions as listed in

Table S1 in the supporting information. (We note that reprocessing the observations of this baseline since 2015 from visibility data will produce four more years of usable observations.) The results from the analyses of not estimating dZWDs for this baseline are presented here, whereas the results of estimating them will be discussed in Sect. 5. The mean number of total observations in these 107 sessions is 302, and the mean number of used observables in the solutions is 276 and 277 for group delay analyses and phase delay analyses, respectively. The mean value of the WRMS delay residuals is 15.6 ps for group delay analyses and 3.9 ps for phase delay analyses. They are approximately at the same level as those determined by the closures of the triangle formed by the Onsala antennas.

The mean formal errors of the estimates of the baseline vector in the east, north, and up directions are 0.6, 0.6, and 1.3 mm from group delay observables, respectively, and they are 0.2, 0.1, and 0.3 mm from phase delay observables. Because the estimates from different sessions are scattered more than one would expect from their formal errors, the formal errors were inflated by introducing a constant additive uncertainty such that the reduced χ^2 of the time series of each coordinate component becomes unity. The additive uncertainty is an indication of the systematic error level in the results that is not measured by the (original) formal error. They are 0.8, 2.5, and 2.3 mm for the three position components from group delay analyses, and 0.3, 0.3, and 0.7 mm for phase delay analyses, respectively. The results suggest that the sub-millimeter accuracy can be achieved for all the three components of this short baseline by phase delays in a single 24-hour session with the S/X observing mode.

We used the inverse of the sum of the squares of the formal error and the additive uncertainty as the relative weight for each individual estimate from one session in calculating the weighted mean baseline vector and the repeatability. The weighted mean of the baseline vector estimates from both group delays and phase delays are presented in Table 2. The baseline vector repeatabilities are 0.3, 0.3, and 0.8 mm from phase delay analyses and 1.1, 2.6, and 3.0 mm from group delay analyses. The precision obtained for this 123 m baseline based on phase delays is likely to demonstrate the best performance that the geodetic VLBI system with the S/X observing mode is capable of. The repeatabilities of the position of `WETTZELL` based on group delays in the 24-hour global sessions are 3, 5, and 9 mm according to the IVS internal report of the ITRF2020 on the 20th IVS analysis workshop in September 13, 2021.

The residuals of the baseline vector estimates from both phase delays and group delays are shown in Fig. 4. There is a significant difference in the up direction between group delay and phase delay results; the weighted mean of the up estimates from group delays is lower than that from phase delays by 1.7±0.2 mm. The distribution of the residuals in the horizontal plane is shown in Fig. 5. The majority of the east and north residuals from the phase delay analyses are within ±0.5 mm. The residuals from group delay analyses systematically spread in the north direction, but they do not show a temporal dependence. The results from group delays in the 24-hour global sessions also have a larger scatter in the north direction than in the east direction as shown in the IVS internal report of the ITRF2020. The differences in the mean horizontal components between group delay results and phase delay results are within three times the uncertainties of the group delay results.

Complementary to the 24-hour sessions, Intensive sessions have been carried out since 1984 (Robertson et al., 1985) to rapidly determine Earth's highly variable phase of rotation. They last for one hour and currently are observed every day by two globally spaced antennas, generally `WETTZELL` and `KOKEE`, and every Monday by more than two antennas including `WETTZELL` and `WETTZ13N`. Due to continuous improvements in VLBI antenna sensitivities and in scheduling (see, e.g., Baver & Gipson, 2020; Schartner et al., 2021), and taking advantage of the consequent more even distribution of usable radio sources on the sky, it has become possible to estimate relative positions for the co-

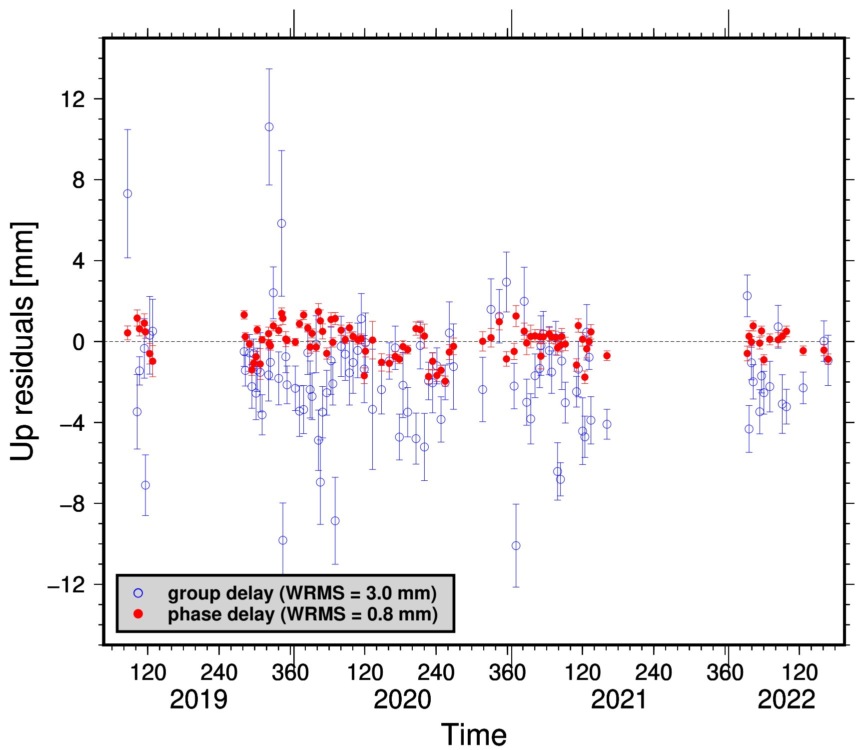

Figure 4. Residuals of the estimated up coordinates of baseline vector `WETTZ13N`–`WETTZELL` from group delay observables (blue open circles) and phase delay observables (red closed circles) based on geodetic analyses of 107 global 24-hour sessions. The error bars are the formal errors of the estimates from geodetic analyses.

Table 2. Weighted mean estimates of the baseline vectors, in geocentric (XYZ) and topographic (ENU) coordinate systems, for the four baselines that have data of more than two VLBI sessions (units: mm). The topographic coordinate system in this work is defined to be centered at the position of the first antenna of a baseline. The baseline vector `WETTZ13N–WETTZELL` from local survey is reported for comparison. L is baseline length with uncertainty σ_L.

Baseline	Observable	X	σ_X	Y	σ_Y	Z	σ_Z	L[1]	σ_L
`Wn–Wz`	Group delay	−88034.29	0.26	−38730.62	0.08	77165.27	0.26	123306.83	0.24
	Phase delay	−88035.64	0.06	−38730.82	0.03	77164.15	0.05	123307.14	0.03
	Local survey	−88036.3	0.49	−38731.5	0.47	77162.8	0.52	123307.0	0.50
`Ns–Ny`	Group delay	1391812.79	0.88	605228.09	0.50	−256274.30	3.81	1539193.64	0.41
	Phase delay	1391815.79	0.28	605228.50	0.28	−256258.16	1.15	1539193.54	0.21
`Is–Ts`	Group delay	2226595.94	0.84	13403264.28	0.56	−9547965.53	0.94	16606290.08	0.53
	Phase delay	2226601.17	0.56	13403259.09	0.44	−9547970.00	0.55	16606289.11	0.24
`Hh–Ht`	Group delay	48041.29	0.86	−102300.32	0.59	4125.36	0.66	113094.39	0.53
	Phase delay	48042.17	0.63	−102300.89	0.18	4126.25	0.63	113095.28	0.30

Baseline	Observable	E	σ_E	N	σ_N	U	σ_U
`Wn–Wz`	Group delay	−18136.24	0.10	121917.55	0.25	−3422.47	0.27
	Phase delay	−18136.08	0.03	121918.05	0.03	−3424.22	0.08
	Local survey	−18136.6	0.47	121917.8	0.50	−3425.8	0.51
`Ns–Ny`	Group delay	306380.24	0.48	−1508019.93	0.44	33575.12	3.84
	Phase delay	306380.05	0.30	−1508019.81	0.26	33591.55	1.14
`Is–Ts`	Group delay	−11725044.07	0.31	−11759335.74	0.50	−101167.29	1.24
	Phase delay	−11725043.48	0.21	−11759334.70	0.23	−101175.48	0.84
`Hh–Ht`	Group delay	−112908.81	0.53	1532.81	0.50	−6289.81	1.02
	Phase delay	−112909.85	0.33	1533.84	0.44	−6289.73	0.74

[1] Baseline length L is derived as the mean of the baseline length estimates over multiple sessions in the same way as for the three position components; therefore, there can be a discrepancy of a few tenths of millimeter between the reported L and the value that one can calculate from the root of the sum of the squares of the three position components. Uncertainty σ_L is calculated from the time series of the baseline length estimates as the uncertainty of the mean value instead of doing error propagation from the uncertainties of the three position components. This process provides an evaluation of baseline length as an independent quantity and is used in the study for these four baselines.

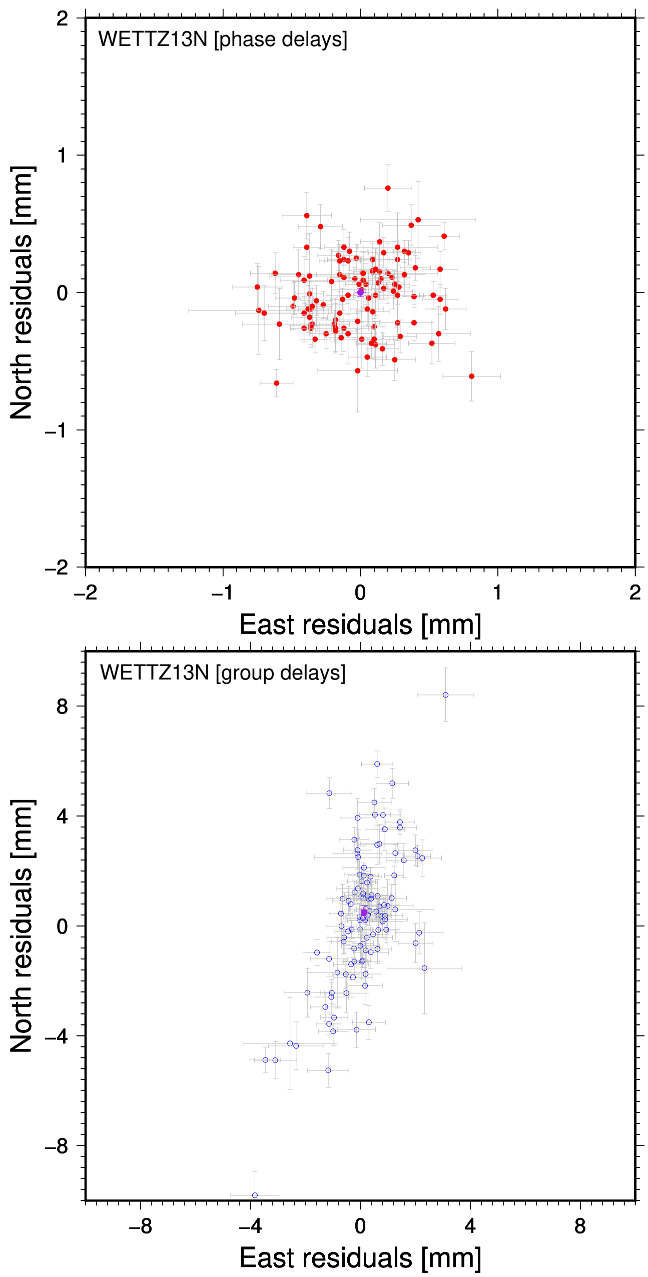

Figure 5. Residuals of the position estimates of baseline `WETTZ13N`–`WETTZELL` in the horizontal plane from group delays (bottom) and phase delays (top) in the 107 global 24-hour sessions. The residuals in both plots are relative to the weighted mean position from phase delays. The weighted mean of the residuals is marked as a purple dot in both plots. Note the different scale.

located pair WETTZELL and WETTZ13N from the Intensive sessions. We use the Intensive sessions here to learn how well the short baseline vector can be determined from one-hour observations by comparing to the results obtained from 24-hour observations.

We have processed 58 Intensive sessions that included the WETTZ13N–WETTZELL baseline within the same time period as the 24-hour sessions, listed in Table S2 in the supporting information. These Intensive sessions on average consist of 43 scans, and the mean number of usable observables of the baseline is 39.0 and 39.6 for group delay and phase delay, respectively. They are at least twice the average numbers per hour of 24-hour sessions. In the data analysis of the Intensive only six parameters are set up: three for the baseline vector and three for the clock. The means of the WRMS delay residuals are 9.5 ps for group delay analyses and 3.1 ps for phase delay analyses, which are significantly smaller than those of the solutions based on the 24-hour sessions. However, since the Intensive sessions do not have significantly higher signal to noise ratio than the regular IVS global 24-hour sessions, these smaller delay residuals in the Intensive sessions may indicate that the shorter sessions are over-parameterized.

The residuals of the position estimates from the Intensives with respect to the reference position obtained from 24-hour sessions are shown in Fig. 6. The mean of the residuals from phase delays is -0.19 ± 0.16 mm, -0.23 ± 0.14 mm, and 0.20 ± 0.17 mm in the east, north, and up directions, respectively; they are 0.07 ± 0.44 mm, -0.19 ± 0.51 mm, and 0.71 ± 0.60 mm for group delays. The formal errors of the position estimates based on phase delays are on the level of $0.6, 0.6,$ and 0.8 mm for the three components, respectively; the additive uncertainties to these formal errors are $1.0, 0.8,$ and 1.0 mm in order to get the χ^2 of the residual time series being unity. The differences in the mean positions between the one-hour observations and the 24-hour observations are not significant with respect to their uncertainties. However, the position residuals show systematic variations, mainly in southwest and northeast as shown in Fig. 6. The phase delay analyses produce a baseline vector repeatability of $1.3, 1.1,$ and 1.3 mm, and the group delay analyses result in $3.4, 4.0,$ and 4.5 mm. Phase delays on a short baseline in an Intensive session have a capability of determining baseline vectors at the 1 mm level.

3.1.2 NYALE13S–NYALES20

The legacy antenna NYALES20 in Norway has an observing history of about 30 years, and it is still one of the most active geodetic stations. The new antenna NYALE13S has participated in the IVS sessions since early 2020 and operated through a series of shakedown experiments; the legacy antenna NYALES20 observed many sessions in 2020 and 2021 with a warm receiver. Thus, the observations of this baseline often have large noise contributions. Due to the large measurement noise and the poor a priori position of the new antenna, it can be challenging to eliminate the phase ambiguities for this baseline. We have 19 sessions available for this baseline to perform both phase delay and group delay analyses. The atmospheric effects were modeled as a PWL function with an interval of one hour in the data analyses of this 1.5 km baseline. The number of the used observables and the WRMS delay residuals based on two types of observables are reported in Table S3 in the supporting information. The mean of the WRMS delay residuals from the IVS reports of the routine data analysis, labeled as 'S/X band delays' in the table, is 53 ps for on average 220 used observables, and the residuals are significantly larger than the typical measurement noise level in the geodetic observations. By removing the involvement of the S band observables in the analyses, labeled as 'Group delays' in the table, the number of usable observables increased by 34%, and the mean of the WRMS delay residuals decreased to 35 ps. A significant improvement has been obtained by using group delays at X band. The mean of the WRMS phase delay residuals is about 16 ps, a significant decrease from the group delay value.

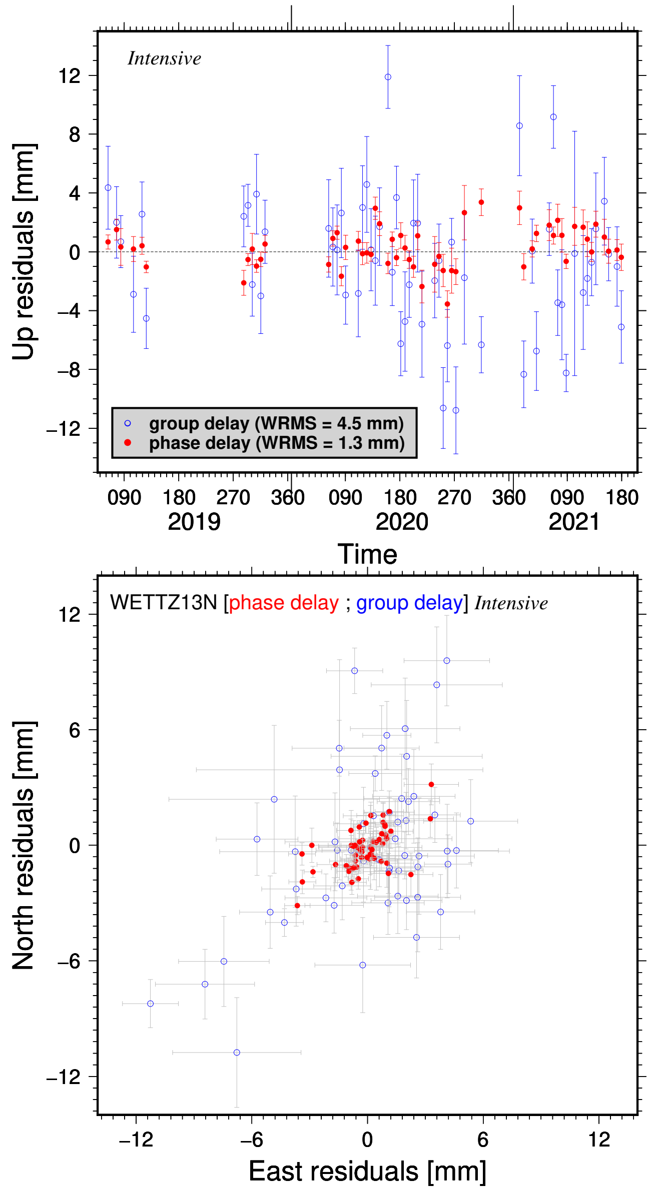

Figure 6. Residuals of the up component (top) and the east and north components (bottom) of baseline vector `WETTZ13N`–`WETTZELL` estimates from 58 Intensive sessions, relative to the weighted mean position from phase delays in 24-hour sessions reported in Table 2. Note the different scale compared to the residual scatter shown in Fig. 5.

The weighted mean estimate of the baseline vector calculated as the mean estimate is reported in Table 2. The phase delay results yield a baseline vector repeatability of 1.3, 1.1, and 4.7 mm, and the group delay analyses yield 2.0, 1.8, and 16.0 mm. The repeatability determined by group delays in the up direction is one order of magnitude larger than that in the horizontal directions, which means that either the large noise level in group delays has a larger impact on the up direction or the large noise in the group delays are not purely random but includes some systematic errors. As the group delays of this baseline obtained based on manual phase calibration have a significantly lower noise level than those based on phase calibration signals, the issues in the group delay results may be due to the phase calibration systems. Referring to the mean position from phase delays, the residuals are shown in Fig. 7 for both phase delays and group delays. The difference between the mean estimates from group delay analyses and phase delay analyses is within the uncertainties of the group delay results in the horizontal plane and about four times the uncertainty in the up direction.

3.1.3 ISHIOKA–TSUKUB32

The new antenna `ISHIOKA` can observe with both the S/X and the VGOS mode, thanks to the interchangeable S/X band and broadband receivers. The 32 m antenna `TSUKUB32` ended observing in December 2016, and it was dismantled in 2017. It is only possible to derive the position tie for this 16.6 km baseline by analyzing historical observations. The reported results of this baseline are from estimating the dZWDs with an interval of one hour. The phase delays in the 17 sessions listed in Table S4 in the supporting information produce a baseline vector repeatability of 0.9, 0.9, and 3.4 mm, and the group delays give 1.2, 2.0, and 4.7 mm. The reference position and the mean position from group delay analyses are listed in Table 2. The difference between the group delay and phase delay results is 8.2 mm in the up direction, significant at the 5-sigma level, and is about 1 mm in the horizontal plane.

3.1.4 HARTRAO–HART15M

Because the frequency standard of antenna `HART15M` was tuned down by $\sim$4.5 Hz, this short baseline has usable observables without applying the notch filter in correlation. The solutions based on the phase delays of this baseline are only slightly better than the ones based on group delays as indicated by the WRMS delay residuals in Table S5 in the supporting information. The mean estimates of the baseline vector from phase delays and group delays in the eight sessions are presented in Table 2. The differences between the results from the two types of observables are not significant with respect to their uncertainties.

3.2 Baselines with only one or two global sessions

The results of the baseline vectors from phase delays for the baselines with only one or two global sessions available are reported in Table 3. The VLBI data for the baseline `SESHAN13`–`SESHAN25` are from session AOV056 (February 03, 2021), and the data for the other six baselines are from two mixed sessions, RD2005 (June 24, 2020) and RD2006 (July 08, 2020). The detail of the data analysis of these observations are presented in the supporting information.

4 Comparison of the results

Local survey measurements have been carried out at the Wettzell site to obtain the baseline vectors with an uncertainty of about 0.5 mm in each of the three components. The local-survey result of the baseline vector `WETTZ13N`–`WETTZELL` is reported in Table 2. This result was derived from the local tie measurements over the course

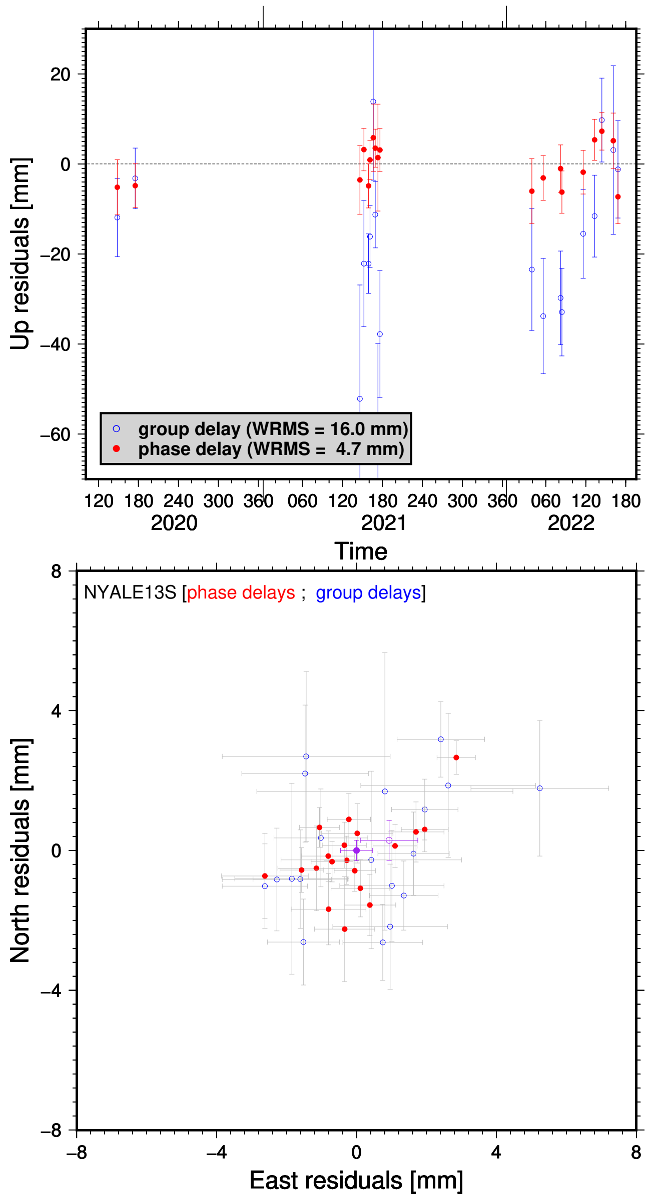

Figure 7. Residuals of the Up component (top) and the east and north components (bottom) of baseline vector `NYALE13S`–`NYALES20`. The residuals are drawn by blue open circles for group delay results, and by red closed circles for phase delay results. The weighted means of the residuals are marked as purple dots in the bottom plot.

Table 3. Estimates of the baseline vectors, in geocentric (XYZ) and topographic (ENU) coordinate systems, for the seven baselines that have only one or two VLBI sessions (units: mm). L is baseline length with uncertainty σ_L. The results are from geodetic solutions based on phase delays. The baseline vector `WETTZ13S–WETTZELL` determined from the local survey measurements is reported.

Baseline	Session	X	σ_X	Y	σ_Y	Z	σ_Z	L	σ_L
`S6–Sh`	AOV056	−40596.42	0.58	3901.92	0.51	−37658.70	0.45	55511.01	0.42
`Ws–Wz`	RD2005	−119342.49	0.28	−89237.27	0.18	113297.05	0.32	187195.46	0.18
	RD2006	−119345.03	0.34	−89238.05	0.22	113293.70	0.41	187195.43	0.22
	Local survey	−119344.4	0.41	−89236.0	0.38	113294.3	0.43	187194.4	0.41
`Yj–Ys`	RD2005	−69291.94	0.54	145344.50	0.33	108556.53	0.55	194192.99	0.35
`K2–Kk`	RD2006	−6068.11	0.23	19214.95	0.17	23720.61	0.17	31124.00	0.14
`On–Ow`	RD2005	340935.36	0.20	−383169.93	0.16	−169947.25	0.25	540313.04	0.16
	RD2006	340935.31	0.23	−383170.17	0.15	−169947.31	0.31	540313.20	0.17
`Oe–On`	RD2005	−283454.24	0.19	346477.62	0.16	138824.67	0.25	468684.69	0.15
`Oe–Ow`	RD2005	57480.67	0.09	−36692.52	0.07	−31123.37	0.13	74960.20	0.07
		E	σ_E	N	σ_N	U	σ_U		
`S6–Sh`	AOV056	32703.72	0.30	−44832.37	0.39	1413.22	0.65		
`Ws–Wz`	RD2005	−60393.44	0.17	177152.60	0.18	−3424.98	0.39		
	RD2006	−60393.63	0.22	177152.42	0.23	−3429.24	0.48		
	Local survey	−60391.8	0.38	−177152.0	0.42	−3428.1	0.42		
`Yj–Ys`	RD2005	141400.02	0.33	132564.10	0.32	11987.94	0.70		
`K2–Kk`	RD2006	−20126.13	0.14	22345.63	0.12	8019.67	0.28		
`On–Ow`	RD2005	−445354.61	0.12	−305876.39	0.12	−6091.16	0.26		
	RD2006	−445354.81	0.16	−305876.33	0.15	−6091.27	0.36		
`Oe–On`	RD2005	397551.87	0.12	248155.52	0.12	6057.04	0.26		
`Oe–Ow`	RD2005	−47773.49	0.07	−57764.40	0.07	4.55	0.15		

of several years, and thus has no nominal temperature of the local environment. Nevertheless, as we will see in section 5, the baseline vectors among the antennas at the Wettzell site are very insensitive to the thermal expansion on the three antennas. The difference of the baseline vector from phase delays with respect to the local survey is 0.5, 0.3, and 1.6 mm in the east, north, and up directions, respectively, and it is 0.4, 0.2, and 3.3 mm for group delays. The VLBI results do not significantly differ from the local-survey tie in the horizontal directions, but the differences in the up direction are significant. The up component from phase delays is closer to the local survey than from group delays for this baseline. As reported in Table 3, the local-survey tie of another short baseline at Wettzell, `WETTZ13S–WETTZELL`, has a significant difference (at the 3-σ level) in the east direction with respect to the VLBI results, about 1.5 mm. For the 4.3 mm difference in the Up component between the results from the two sessions RD2005 and RD2006, the local survey shows a better consistence with the RD2006 result. The comparisons of these two baselines suggest that the VLBI results and the local survey measurements may have a difference of 1–2 mm in the horizontal directions and up to a few mm in the Up direction.

As mentioned, the results of the short baselines at the Kokee Park and at the Onsala Space Observatory were previously reported by Niell et al. (2021) and Varenius et al. (2021), respectively. Compared with the result of the baseline `KOKEE12M–KOKEE` from VLBI measurements with an mean date of April 11, 2016 (Niell et al., 2021), the change of our result is insignificant in the horizontal directions but has a magnitude of 4.0 mm in the Up direction. For the legacy antenna and the twin VGOS antennas at the Onsala Space Observatory, the difference in the baseline vector `ONSA13NE–ONSA13SW` between our results and that reported in Varenius et al. (2021) is less than 0.2 mm in the horizontal directions and 0.8 mm in the Up direction.

As an independent determination of the baseline vectors at the accuracy of the sub-mm level, our results from phase delays were used to validate the latest realization of ITRF, ITRF2020 (see `https://itrf.ign.fr/en/solutions/ITRF2020`). See Table 4. There are two baselines not listed in the table: `ISHIOKA–TSUKUB32` because of the post-seismic deformation model employed for station `TSUKUB32` in the ITRF2020 but not for station `ISHIOKA` and `SESHAN13–SESHAN25` due to the missing station `SESHAN13` in the ITRF2020. The listed nine baselines all have the position differences larger than 1 mm, even though most of them are consistent with the uncertainties that are dominated by that of the ITRF2020. Two baselines have the differences at the cm level: `NYALE13S–NYALES20` and `RAEGYEB–YEBES40M`. The former baseline vector has only been determined with an accuracy of several centimeters in the ITRF2020 due to the large impact from S band as discussed in sections 2.4 and 3.1.2, and the latter one is most likely affected by the receiver replacement at `YEBES40M` in 2011.

5 Discussion on sources of error

It is worthwhile to note that sub-millimeter repeatability has been demonstrated through short baselines by other space geodetic techniques than VLBI, for instance, the Global Navigation Satellite Systems (GNSS) by Hill et al. (2009); King & Williams (2009). These studies have used the short-baseline time series to investigate the site-specific errors and the stability for GNSS. However, due to completely different data collection and processing methods between the various space geodetic techniques, the sub-millimeter repeatability and the error investigation should be carried out independently for each technique toward the 1 mm accuracy goal of global geodesy.

An early phase delay analysis of eleven VLBI sessions of the 1 km baseline `HAYSTACK–WESTFORD` determined a baseline vector repeatability of 5, 3, and 7 mm in the east, north, and up components (Carter et al., 1980). Then, later with the improved Mark III VLBI system, Herring (1992) obtained a repeatability of 0.8, 0.7, and 2.3 mm

Table 4. Differences of the baseline vector estimates from short-baseline phase delays with respect to the ITRF2020, which are listed in Table S6 in the supporting information (units: mm).

Baseline	Monument	Observable	X	σ_X	Y	σ_Y	Z	σ_Z
Wn–Wz	7387–7224		0.86	1.28	1.08	1.20	1.25	1.50
Ns–Ny	7392–7331		−7.61	25.21	12.50	25.31	5.34	27.44
Hh–Ht	7378–7232		6.37	2.08	1.91	1.64	−2.85	1.94
Ws–Wz	7388–7224	RD2005	0.81	1.63	0.93	1.45	2.25	1.87
		RD2006	−1.73	1.65	0.15	1.46	−1.10	1.89
Yj–Ys	7389–7386	RD2005	26.76	2.36	−0.30	1.54	25.63	2.36
K2–Kk	7623–7298	RD2006	7.79	3.90	−3.55	2.97	−2.09	3.45
On–Ow	7213–7637	RD2005	1.06	2.95	−0.43	1.98	−1.35	4.52
		RD2006	1.01	2.95	−0.67	1.98	−1.41	4.52
Oe–On	7636–7213	RD2005	1.26	2.48	0.42	1.80	4.47	3.55
Oe–Ow	7636–7637	RD2005	1.87	3.62	−0.22	2.41	2.33	5.56

for the same baseline by using phase delays in 24 VLBI sessions. The baseline length of WETTZ13N–WETTZELL is 123 m, one order of magnitude shorter than that of baseline HAYSTACK–WESTFORD; both baselines observed in the S/X mode. As a continuation of the investigations from six sessions of WETTZ13N–WETTZELL in Halsig et al. (2019), which were based on group delays, the larger dataset of 107 global 24-hour sessions and 58 Intensives over 2.5 years and the significantly improved repeatability in our study provide the opportunity to assess the error components more stringently.

What are the important sources of error in the repeatability of the baseline vector estimates of this short baseline? The investigation based on the metric of repeatability in most cases is sufficient for geophysical and astrophysical studies, such as a change in the orientation of the Earth in space and the station position variations due to tidal displacements or tectonic motions. However, some of the instrumental effects can be highly repeatable and thus are not detected by the WRMS scatter of the estimates. It is necessary to also investigate those repeatable errors in the VLBI system itself for the purpose of combining the station positions from various space techniques for the realization of ITRF. Therefore, which of these error components are repeatable (related to accuracy) or not repeatable (precision)? We devote this section to addressing these questions.

(1) *Measurement noise in delay observables* The uncertainty of a baseline vector estimate due to measurement noise in observables generally manifests itself as the formal error from the geodetic solution based on least square fitting (LSF). A session-wise delay noise was added in quadrature to the uncertainties of the observables in LSF to account for potential systematic errors already at the observation level. And in fact, the additive noise is comparable to the corresponding WRMS delay residual as shown in Table S2 in the supporting information. Therefore, the uncertainty due to measurement noise is lower than the formal error of the estimate by a factor of approximately $\sqrt{2}$. Taking this factor into account, the impact of measurement noise in

phase delays on the baseline vector of WETTZ13N–WETTZELL is 0.1 mm on the horizontal plane and 0.4 mm in the up direction, and for group delays it is 0.5 mm and 2.0 mm.

(2) *Cable delays* The time delays of the astronomical signal passing through the electronic devices within the antennas are expected to be smoothly varying and are absorbed in the clock parameters. In order to eliminate their variations, phase calibration systems are used to correct the visibility phases. Meanwhile, the time delays through the cable that carries the precisely timed pulses from the frequency standard to the injection of phase calibration signals are actually not experienced by the astronomical signals; these cable delays are measured as corrections to be applied in geodetic solutions. Of the eleven baselines in this study, only KOKEE12M–KOKEE, RAEGYEB–YEBES40M, WETTZ13S–WETTZELL, and the baselines formed by the Onsala antennas have the cable delay corrections available for both antennas. In fact, proxy corrections for KOKEE12M instead of direct measurements were used (see, Niell et al., 2021), and the cable delay corrections of antenna RAEGYEB were not applied for the final solution. It is possible that variations of the time delays in the antenna electronics and cabling cause significant impacts due to the missing corrections for some antennas.

We ran geodetic solutions of the 107 sessions in which the cable delay corrections of antenna WETTZELL were not applied by intention. We must emphasize that turning off the cable delay corrections did not degrade the solutions in the sense of the WRMS delay residuals and the baseline vector repeatability when comparing to the solutions with the corrections applied. After turning off the cable delay corrections of antenna WETTZELL, the mean of the changes in the baseline vector estimates from phase delays is 0.23 ± 0.03 mm, 0.07 ± 0.02 mm, and 1.65 ± 0.11 mm in the east, north, and up directions, respectively. As discussed in the supporting information, the cable delay corrections of antenna RAEGYEB have an impact of about 6 mm on the up direction. For the ONSALA60 antenna, the impact is estimated to be dominant also in the up direction, which is even at the level of 1 cm (Varenius et al., 2021). The uncertainty due to missing cable delay calibrations may be at the sub-millimeter level on the horizontal directions and a few millimeters or larger in the up direction. The impact is repeatable at the 0.1 mm level for antenna WETTZELL. This repeatable feature may affect other antennas if the distribution of the elevation and azimuth angles does not change dramatically from session to session such that the cable is twisted in the same manner.

(3) *Antenna thermal expansion* The antenna structure experiences thermal deformation, and this leads to station position changes due to the temperature variations at the site. This effect and the models have been well studied (see, e.g., Nothnagel, 2009, and the references therein). The antenna-dependent parameters in these models are maintained and publicly available for most of the geodetic antennas (from `https://raw.githubusercontent.com/anothnagel/antenna-info/master/antenna-info.txt`). However, the practical problem of applying these models at the observation level in geodetic solutions can be that the desired temperatures of the antenna structural elements are specific functions of the time history of the ambient temperatures. Therefore, the information of these temperatures are not complete in VLBI databases. Nevertheless, the mean temperature during the 24 hours of observations would not significantly differ from the mean value of the temperatures that actually cause the thermal expansion. We use the temperatures recorded at the same epochs of observations in a session to derive the mean value and assess this source of error accordingly.

The temperature dependence of antenna thermal expansion consists of constant terms and elevation-dependent terms. In the case of WETTZ13N and WETTZELL, which have zero axis offsets, the elevation-dependent terms are proportional to the sine of the elevation angle. The extra path length due to the thermal expansion mimics exactly the effect of a vertical displacement of the antenna. The relative foundation height of WETTZ13N minus WETTZELL is -2 m with an expansion coefficient of 1.0×10^{-5} per °C, and the relative height of the supporting axes is $+1$ m with an expansion coefficient of

1.2×10^{-5} per °C. Therefore, an increase of 1°C at the site will cause the up component of WETTZ13N's position (relative to WETTZELL) to decrease by 0.008 mm. Based on the meteorological data recorded at each observation epoch, the median value of the mean temperatures in these sessions is 7.7°C, which is very close to the reference temperature of the model parameters previously mentioned. The rms scatter of the temperatures within one session has a median value of 2.3°C; thus, the impact due to the temperature variations within a day is negligible. There is a seasonal variation in the mean temperatures with an amplitude of 11.5±0.7 °C. Even though the actual variations due to this effect will be about −1.4 mm in winter and about +1.4 mm in summer for both antennas, the corresponding impact on the baseline vector of WETTZ13N–WETTZELL has a magnitude of only 0.1 mm in the up component.

For baseline ONSALA60–ONSA13SW from June 24 to July 08, 2020, the impact of thermal expansion is about 0.2 mm in the up direction due to the temperature change of 5.2°C at the site. We also note that the temperatures can be different between these two antennas because ONSALA60 is enclosed in a radome. Nevertheless, the impact of this effect cannot explain the difference in the estimates of the up component of this baseline vector from the two sessions, as presented in Table 3. The impact of thermal expansion is typically very small (i.e., below 1 mm) for the short baselines except RAEGYEB–YEBES40M, since the temperature is close to the same for multiple antennas at a site and they tend to have similar physical dimensions. This source of error should show a seasonal variation in the up direction.

(4) *Antenna gravitational deformation* In contrast to the constant, known coefficients of thermal expansion, the gravitational deformation of the main reflector and its distance to the secondary reflector needs to be measured individually for each antenna. Extensive measurements of this effect for the Onsala antennas have been made by employing other measuring techniques (see, e.g., Nothnagel et al., 2019; Bergstrand et al., 2019; Lösler et al., 2019). These studies demonstrated that the effect produces systematic offsets in the up component of the position of the 20 m Onsala antenna of about 1 cm; however, the change is smaller than 1 mm for the 13.2 m VGOS antennas at the site. These results may be considered representative of the impacts on the legacy antennas and the VGOS antennas at the other geodetic VLBI sites. The IVS recently adopted the resolution of every radio telescope operating in IVS observing sessions being surveyed for gravitational deformation investigations (see https://ivscc.gsfc.nasa.gov/about/resolutions/IVS-Res-2019-01-TelescopeSurveys.pdf).

The extra raypath introduced by antenna gravitational deformation is a smooth curve with respect to elevation angle, as measured for ONSALA60, similar to a sine function. Therefore, the major impact on station position estimates is on the up component, as shown in the data analysis of Varenius et al. (2021). If this elevation dependence were exactly a sine function, the impact would again be equivalent to a displacement in the up position with a magnitude of the gravitational deformation at zenith direction. Moreover, regardless of whatever is the exact form of the elevation dependence, the impact on position estimates is repeatable as long as the elevation angles have a similar distribution from one session to another. This is valid for baseline WETTZ13N–WETTZELL, because there is no significant difference in the scheduling of the 107 sessions with the same goal — only four of the 107 sessions are for the determination of TRF and the other 89 are R1 and R4 sessions. Nevertheless, we might conclude that the non-repeatable component of the antenna gravitational deformation is likely smaller than the repeatability of the baseline vector WETTZ13N–WETTZELL.

Since the gravitational deformation of the VGOS antennas is measured to be below 1 mm (though to be measured and confirmed for more VGOS antennas), an order of magnitude smaller than that of the legacy antennas, the corresponding error for VGOS is expected to be smaller than that of baseline WETTZ13N–WETTZELL.

(5) *Antenna tilt* It is possible that the supporting axis of an antenna tilts toward a direction in the horizontal plane as time goes on (Niell et al., 2021). Based on the 3.5 years of observations of WETTZ13N–WETTZELL, however, the horizontal motion is determined to be negligible, -0.02 ± 0.04 mm/yr and -0.03 ± 0.03 mm/yr in the east and north directions, respectively.

(6) *Signal chain* Due to the large systematic differences in group delay and phase delay observables as shown in Fig. 2, we believe that there is a possibility of significant errors introduced in the signal chain before the injection of phase calibration signals or due to spurious phase calibration signals (see, Rogers, 1991). As we have stated, a large fraction of the systematic differences between group delay and phase delay observables attributes to group delay observables. It is important to identify the causes of these systematic differences, as group delays are the basic observables of geodetic VLBI. However, any conclusion on this effect needs further investigations.

(7) *Polarization-related effects* The polarization leakage (Martí-Vidal et al., 2021) can have different impacts between the observations of the legacy S/X and the mixed modes. The visibility of $RH+RV$ from the mixed mode session is not able to minimize the impact of the D term as is the pseudo-Stoke I visibility constructed for the dual linear polarizations in VGOS; without being calibrated, there may be significant errors. However, the short baselines with more than two sessions available were observed in the legacy S/X mode. The results so far do not allow us to assess the potential errors in the mixed mode of the circularly polarized receivers and the linearly polarized receivers. The only information that we presently have is that the residual level of the mixed mode observables of baselines ONSALA60–ONSA13NE and ONSALA60–ONSA13SW is about 5.0 ps and that of baseline ONSA13NE–ONSA13SW, both of which observed with the linearly polarized receivers, is only 2.0 ps based on the data analyses of the two mixed mode sessions. However, the former two baselines are about five times longer, which prevents us from making any conclusion so far. We leave these effects for a later investigation.

(8) *Source positions* The short baselines in this study are sensitive to source structure only at the sub-arcsecond level or larger, three orders of magnitude greater than the typical uncertainties of source positions in the third realization of the International Celestial Reference Frame (ICRF3; Charlot et al., 2020). In general, source positions are not estimated in data analysis of short-baseline observations, as one would keep the number of model parameters to a minimum to obtain robust solutions. Due to radio interferometry, source structure at the arc-second scales is resolved out and not detected by the long baselines of thousands of kilometers. The source positions in the ICRF3, determined primarily from long-baseline observations, were used as a priori and not estimated in our solutions. However, the ICRF3 source positions can be different from the reference positions for the short baselines due to large scale structure for some of the sources. Even though we have stated that these effects should be small for most of the geodetic sources, the magnitude should be properly quantified by actual observations.

We analyzed the VLBI sessions of station position tie carried out at the Onsala site, the ONTIE sessions (Varenius et al., 2021). The advantages of these ONTIE sessions for this particular investigation are the large number of scans ($\sim$1200 scans per session) and the multiple short baselines formed by the three antennas at the site; they allow us to obtain robust solutions for estimating a large number of source position parameters. For instance, session 20NOV12VB observed 126 sources with 3522 observations in total. With the parameterization of one-hour-interval PWL functions for both the dZWDs and the clocks of antennas ONSA13NE and ONSA13SW and the positions of the two antennas, the WRMS delay residual is 2.9 ps based on 3442 used phase delays. The formal errors of station position estimates are 0.2 mm in the up direction and 0.05 mm in the horizontal directions. In another solution, we estimated right ascension and declination for the 105 sources with more than ten phase delays together with the same parameters in the previous solution. The WRMS delay residual is 2.7 ps from the solution of estimating source positions; however, the formal errors of station position estimates increase by 50% in the up direction and by 100% in the horizontal directions. The differences in station position estimates are about 0.1 mm in the up direction and 0.2 mm in the two horizontal directions, a demonstration that errors in source positions affect the horizontal directions rather than the up direction for the ties. The results from other ONTIE sessions are similar to that of session 20NOV12VB presented here. Radio sources observed in the ONTIE sessions are from the same source catalog of the IVS observations; thus, it is reasonable to conclude that the impact of source position differences due to large scale structure may be about 0.2 mm on the horizontal directions. This is insignificant relative to the uncertainties and probably will not cause systematic changes in position estimates but only increase the scatters. There is no intention either to observe the same set of sources or to observe a given source at the same Greenwich mean sidereal time in different sessions, therefore, this error source is non-repeatable (i.e., a random error as opposed to a systematic error).

(9) *Atmospheric effects* In order to separate the elevation-dependent effects of the atmosphere from the estimates of station positions, in particular the Up component, geodetic VLBI observations rapidly switch between radio sources at different directions. Fortunately, atmospheric effects are greatly canceled for short baselines and the hydrostatic part of the effects is modeled in our solutions. The residual effects are investigated and discussed here.

Based on phase delays of `WETTZ13N–WETTZELL` in the 107 sessions, we performed three sets of solutions: (1) estimating dZWDs with a time interval of PWL of 1 hour, (2) estimating dZWDs with a time interval of 24 hours, and (3) not estimating dZWDs. Differences in the mean estimates of the horizontal components are negligible, smaller than 0.01 mm, between these three sets of solutions, and the mean of the differences in the Up component is 0.05 ± 0.05 mm between estimating dZWDs with two different time intervals. However, the mean of the differences in the Up estimates between estimating dZWDs (with a time interval of either 24 hours or 1 hour) and not estimating is -1.1 ± 0.1 mm. The residual time series of the Up estimates from the three sets of solutions are shown in Fig. 8. Seasonal variations with a magnitude larger than 1 mm occur in the Up residuals when the dZWDs were estimated. Even though the atmospheric turbulence due to wet troposphere on the local scale is believed to have detectable effects in VLBI observables (see, e.g., Treuhaft & Lanyi, 1987), our results suggest that the baseline time series can be stabilized by not estimating the atmospheric effects in the case of the short baseline `WETTZ13N–WETTZELL`. Through the investigation, we conclude that the impact of atmospheric effects on the baseline ties from short-baseline observations is negligible in the horizontal components but can be 1–2 mm in the Up component. This amount of impact may be inevitable and prevalence in the current VLBI products because the signal propagation delays due to water vapour are always estimated in geodetic solutions of VLBI observations. The study may suggest that achieving global geodetic accuracy of 1 mm with VGOS will have to reply on corrections for the water vapour-induced delays from independent instruments, such as collocated microwave radiometers (see, e.g., Forkman et al., 2021).

6 Potential applications of phase delays from long baselines

We have demonstrated that phase delays can be used (1) to investigate the systematic errors of group delays and (2) to derive geodetic results of baseline vectors. However, the study has limited to utilizing these observables from short baselines, mainly due to the challenge in resolving phase ambiguities for long baselines. In this

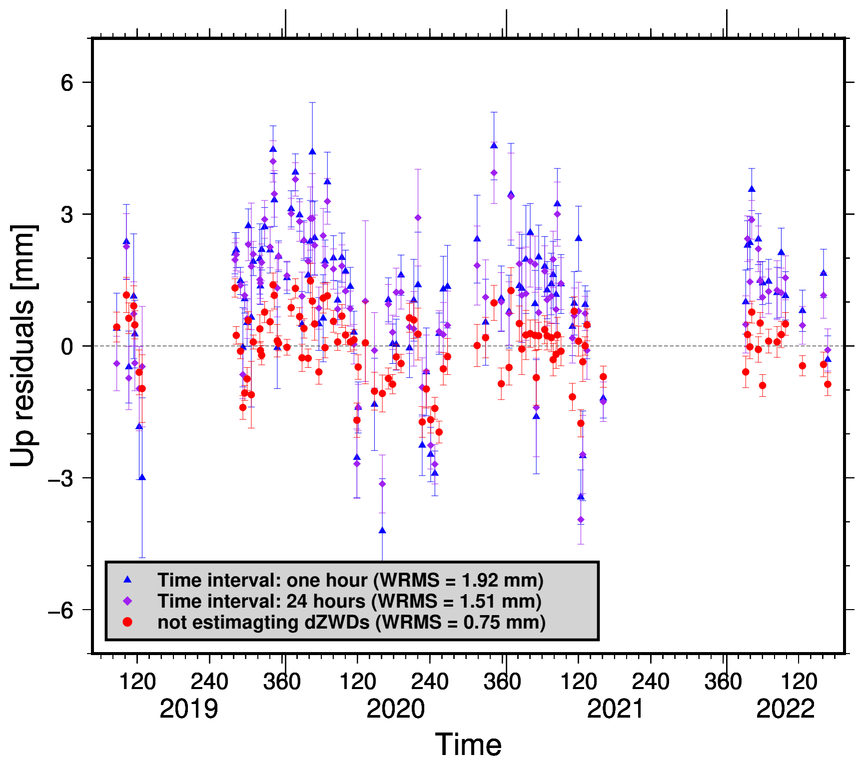

Figure 8. Comparison of the Up residuals from solutions with three different treatments of the atmospheric effects: estimating with a time interval of 1 hour for PWL (blue triangles), estimating with a time interval of 24 hours (purple rhombuses), and not estimating (red dots). The black dash line indicate the mean Up position obtained from the solutions without estimating ZWDs, which is the reference for calculating the Up residuals of all the three types of solutions.

section, we will briefly discuss the potential application of phase delays from long baselines.

As discussed in section 2.2 in detail, the methods of resolving phase ambiguities include: (1) directly employing group delays to predict the phase ambiguities, (2) using theoretical model delays, and (3) relying on geodetic solutions of group delays. Because typically instrumental effects can introduce large systematic errors in the ionospheric corrections determined from S/X-band group delays (e.g., constant offsets) and resolving phase ambiguities for long baselines requires a special attention to the difference in the reference frequencies of these corrections between group delays and phase delays (e.g., the constant offsets can introduce large variations due to the changes in the reference frequencies of the corrections from group delays), neither of these three options could work well for long baselines in the legacy VLBI observations. In the VGOS observations, however, because the ionospheric effects are simultaneously estimated with group delays and visibility phases in the broadband fringe fitting process (Cappallo, 2014), this naturally resolves the challenge of predicting phase ambiguities caused by the ionospheric effects. The VGOS phase delays are recently discussed and investigated by the IVS VGOS Technical Committee, and their potential applications can be to improve the quality of the group delays and to investigate the effects of source structure (Xu et al., 2022) with the goal of improving the geodetic products from VGOS. We remark that without mitigating the systematic errors caused by, e.g., water vapour and source structure, the higher precision of phase delays alone cannot promise significantly better geodetic products in general cases of long baselines.

7 Summary

We have analyzed the phase delays in the IVS routine global observations for the short baselines at eight geodetic VLBI sites to derive the station position ties with high accuracy. The results of the baseline vector `WETTZ13N–WETTZELL` have baseline repeatabilities of better than 1 mm in all the three directions. The potential systematic errors were investigated and discussed in the study. As demonstrated by the investigation of the cable delay corrections, instrumental effects typically can introduce errors with a magnitude larger than 1 mm in station position estimates. The atmospheric effects, which are always estimated in geodetic solutions, may also cause seasonal fluctuations at the a few mm level in station position time series.

Phase delays produce significantly better determinations of the baseline vectors than the linearly combined group delays at S/X bands. An independent solution of only short-baseline observables does not suffer from some of the errors in long-baseline observables. The phase delay results of the position ties can be directly used in the data analysis of legacy S/X observations and VGOS observations or the combined analysis of both observations. Nevertheless, it should be noted that there currently exists incompatibility in applying these phase delay results to the routine data analysis based on group delays since some antenna pairs have significantly different position ties between group delays and phase delays. When the VLBI phase delay results are used for studies with other space techniques (see, e.g., Ning et al., 2015; Glaser et al., 2019), an attention should be paid to take the systematic, repeatable errors into account, in particular the up coordinate.

Acknowledgments

The results reported in this paper used the data coordinated by the International VLBI Service (IVS) and its international self-funded member organizations. We are grateful to the IVS stations at Hartebeesthoek (South Africa Radio Astronomical Observatory), Ishioka (Geospatial Information Authority of Japan), Kokee Park (U.S. Naval Observatory and NASA GSFC, USA), Ny-Ålesund (Norwegian Mapping Authority, Norway), Onsala (Onsala Space Observatory, Chalmers University of Technology, Sweden), Shanghai (Shanghai Astronomical Observatory, China), Wettzell (Bundesamt für Kartographie und Geodäsie and Technische Universität München, Germany), and Yebes (Instituto Geográfico Nacional, Spain), to the staff at the Bonn Correlator, the Washington Correlator, the Onsala Observatory Correlator, and the MIT Haystack Observatory correlator for performing the correlations and the fringe fitting of the data, to the NASA GSFC VLBI group and the BKG VLBI group for doing the geodetic solutions, and to the IVS Data Centers at BKG (Leipzig, Germany), Observatoire de Paris (France), and NASA CDDIS (Greenbelt, MD, USA) for the central data holds.

This research has made use of the Generic Mapping Tools package, the pgplot library, and the SAO/NASA Astrophysics Data System. The work was supported by the Academy of Finland project No. 315721.

References

Altamimi, Z., Rebischung, P., Métivier, L., & Collilieux, X. (2016). ITRF2014: A new release of the International Terrestrial Reference Frame modeling non-linear station motions. *Journal of Geophysical Research (Solid Earth)*, *121*(8), 6109-6131. doi: 10.1002/2016JB013098

Anderson, J. M., & Xu, M. H. (2018). Source Structure and Measurement Noise Are as Important as All Other Residual Sources in Geodetic VLBI Combined. *Journal of Geophysical Research (Solid Earth)*, *123*(11), 10,162-10,190. doi: 10.1029/2018JB015550

Baver, K., & Gipson, J. (2020). Balancing source strength and sky coverage in IVS-INT01 scheduling. *Journal of Geodesy*, *94*(2), 18. doi: 10.1007/s00190-020-01343-1

Bergstrand, S., Herbertsson, M., Rieck, C., Spetz, J., Svantesson, C.-G., & Haas, R. (2019). A gravitational telescope deformation model for geodetic VLBI. *Journal of Geodesy*, *93*(5), 669-680. doi: 10.1007/s00190-018-1188-1

Cappallo, R. (2014, Dec). Correlating and Fringe-fitting Broadband VGOS Data. In *International vlbi service for geodesy and astrometry 2014 general meeting proceedings: "vgos: The new vlbi network* (p. 91-96). Retrieved from https://ivscc.gsfc.nasa.gov/publications/gm2014/019_Cappallo.pdf

Carter, W. E., Rogers, A. E. E., Counselman, C. C., & Shapiro, I. I. (1980). Comparison of geodetic and radio interferometric measurements of the Haystack-Westford base line vector. *JGR*, *85*(B5), 2685-2687. doi: 10.1029/JB085iB05p02685

Charlot, P., Jacobs, C. S., Gordon, D., Lambert, S., de Witt, A., Böhm, J., Fey, A. L., Heinkelmann, R., Skurikhina, E., Titov, O. , Arias, E. F., Bolotin, S., Bourda, G., Ma, C., Malkin, Z., Nothnagel, A., Mayer, D., MacMillan, D. S., Nilsson, T. , & Gaume, R. (2020). The third realization of the International Celestial Reference Frame by very long baseline interferometry. *Astronomy and Astrophysics*, *644*, A159. doi: 10.1051/0004-6361/202038368

Forkman, P., Flygare, J., & Elgered, G. (2021). Water vapour radiometry in geodetic very long baseline interferometry telescopes: assessed through simulations. *Journal of Geodesy*, *95*(11), 117. doi: 10.1007/s00190-021-01571-z

Diamantidis, P.-K., Kłopotek, G., & Haas, R. (2021). VLBI and GPS inter- and intra-technique combinations on the observation level for evaluation of TRF and EOP. *Earth, Planets, and Space*, *73*(1), 68. doi: 10.1186/s40623-021-01389-1

Glaser, S., König, R., Neumayer, K. H., Nilsson, T., Heinkelmann, R., Flechtner, F., & Schuh, H. (2019). On the impact of local ties on the datum realization of global terrestrial reference frames. *Journal of Geodesy*, *93*(5), 655-667. doi: 10.1007/s00190-018-1189-0

Halsig, S., Bertarini, A., Haas, R., Iddink, A., Kodet, J., Kronschnabl, G., Neidhardt, A., Nothnagel, A., Plötz, C., & Schüler, T. (2019). Atmospheric refraction and system stability investigations in short-baseline VLBI observations. *Journal of Geodesy*, *93*(4), 593-614. doi: 10.1007/s00190-018-1184-5

Herring, T. A. (1992). Submillimeter horizontal position determination using very long baseline interferometry. *JGR*, *97*(B2), 1981-1990. doi: 10.1029/91JB02649

Hill, E. M., Davis, J. L., Elósegui, P., Wernicke, B. P., Malikowski, E., & Niemi, N. A. (2009). Characterization of site-specific GPS errors using a short-baseline network of braced monuments at Yucca Mountain, southern Nevada. *Journal of Geophysical Research (Solid Earth)*, *114*(B11), B11402. doi: 10.1029/2008JB006027

King, M. A., & Williams, S. D. P. (2009). Apparent stability of GPS monumentation from short-baseline time series. *Journal of Geophysical Research (Solid Earth)*, *114*(B10), B10403. doi: 10.1029/2009JB006319

Lösler, M., Haas, R., Eschelbach, C., & Greiwe, A. (2019). Gravitational deformation of ring-focus antennas for VGOS: first investigations at the Onsala twin telescopes project. *Journal of Geodesy*, *93*(10), 2069-2087. doi: 10.1007/s00190-019-01302-5

Martí-Vidal, I., Mus, A., Janssen, M., de Vicente, P., & González, J. (2021). Polarization calibration techniques for the new-generation VLBI. *Astronomy and Astrophysics*, *646*, A52. doi: 10.1051/0004-6361/202039527

Niell, A., Whitney, A., Petrachenko, W., Schlüter, W., Vandenberg, N., Hase, H., Koyama, Y., Ma, C., Schuh, H., & Tuccari, G. (2007). VLBI2010: a Vision for Future Geodetic VLBI. In P. Tregoning & C. Rizos (Eds.), *Dynamic planet - monitoring and understanding a dynamic planet with geodetic and oceanographic tools, edited by paul tregoning and chris rizos. isbn isbn 978-3-540-49349-5. berlin: Springer, 2007., p.757* (p. 757). Retrieved from https://link.springer.com/chapter/10.1007/978-3-540-49350-1_108

Niell, A. E., Barrett, J. P., Cappallo, R. J., Corey, B. E., Elosegui, P., Mondal, D., Rajagopalan, G., Ruszczyk, C. A., & Titus, M. A. (2021). VLBI measurement of the vector baseline between geodetic antennas at Kokee Park Geophysical Observatory, Hawaii. *Journal of Geodesy*, *95*(6), 65. doi: 10.1007/s00190-021-01505-9

Ning, T., Haas, R., & Elgered, G. (2015). Determination of the local tie vector between the VLBI and GNSS reference points at Onsala using GPS measurements. *Journal of Geodesy*, *89*(7), 711-723. doi: 10.1007/s00190-015-0809-1

Nothnagel, A. (2009). Conventions on thermal expansion modelling of radio telescopes for geodetic and astrometric VLBI. *Journal of Geodesy*, *83*(8), 787-792. doi: 10.1007/s00190-008-0284-z

Nothnagel, A., Artz, T., Behrend, D., & Malkin, Z. (2017). International VLBI Service for Geodesy and Astrometry. Delivering high-quality products and embarking on observations of the next generation. *Journal of Geodesy*, *91*(7), 711-721. doi: 10.1007/s00190-016-0950-5

Nothnagel, A., Holst, C., & Haas, R. (2019). A VLBI delay model for gravitational deformations of the Onsala 20 m radio telescope and the impact on its global coordinates. *Journal of Geodesy*, *93*(10), 2019-2036. doi: 10.1007/s00190-019-01299-x

Petrachenko, B., Niell, A., Behrend, D., Corey, B., Boehm, J., Charlot, P., Collioud, A., Gipson, J., Haas, R., Hobiger, T., Koyama, Y., MacMillan, D., Malkin, Z., Nilsson, T., Pany, A., Tuccari, G., Whitney, A., & Wresnik, J. (2009). *Design Aspects of the VLBI2010 System. Progress Report of the IVS VLBI2010 Committee, June 2009.* NASA/TM-2009-214180.

Phogat, A., Kronschnabl, G., Pltz, C., Schwarz, W., & Schler, T. (2018). Short baseline observations at geodetic observatory wettzell. *Data*, *3*(4). Retrieved from https://www.mdpi.com/2306-5729/3/4/64 doi: 10.3390/data3040064

Ray, J. R., & Corey, B. E. (1991). Current Precision of VLBI Multi-Band Delay Observables. In *Geodetic vlbi: Monitoring global change* (p. 123). Retrieved from https://www.ngs.noaa.gov/PUBS_LIB/Proceedings_of_AGU_Chapman_Conference_on_Geodetic_VLBI_TM_NOS137_NGS49.pdf

Robertson, D. S., Carter, W. E., Campbell, J., & Schuh, H. (1985). Daily Earth rotation determinations from IRIS very long baseline interferometry. *Nature*, *316*(6027), 424-427. doi: 10.1038/316424a0

Rogers, A. E. E. (1991). Instrumentation Improvements to Achieve Millimeter Accuracy (Keynote Presentation). In *Geodetic vlbi: Monitoring global change* (p. 1). Retrieved from https://www.ngs.noaa.gov/PUBS_LIB/Proceedings_of_AGU_Chapman_Conference_on_Geodetic_VLBI_TM_NOS137_NGS49.pdf

Rothacher, M., Angermann, D., Artz, T., Bosch, W., Drewes, H., Gerstl, M., Kelm, R., König D., König R., Meisel H., Müller H., Nothnagel A., Panafidina N., Richter B., Rudenko S., Schwegmann W., Seitz M., Steigenberger P., Tesmer S., Tesmer V., & Thaller, D. (2011). GGOS-D: homogeneous reprocessing and rigorous combination of space geodetic observations. *Journal of Geodesy*, *85*(10), 679-705. doi: 10.1007/s00190-011-0475-x

Schartner, M., Kern, L., Nothnagel, A., Böhm, J., & Soja, B. (2021). Optimal VLBI baseline geometry for UT1-UTC Intensive observations. *Journal of Geodesy*, *95*(7), 75. doi: 10.1007/s00190-021-01530-8

Schuh, H., & Behrend, D. (2012). VLBI: A fascinating technique for geodesy and astrometry. *Journal of Geodynamics*, *61*, 68-80. doi: 10.1016/j.jog.2012.07.007

Schüler, T., Kronschnabl, G., Plötz, C., Neidhardt, A., Bertarini, A., Bernhart, S., la Porta, L., Halsig, S., & Nothnagel, A. (2015). Initial Results Obtained with the First TWIN VLBI Radio Telescope at the Geodetic Observatory Wettzell. *Sensors*, *15*(8), 18767-18800. doi: 10.3390/s150818767

Sekido, M., Takefuji, K., Ujihara, H., Kondo, T., Tsutsumi, M., Kawai, E., Hachisu, H., Nemitz, N., Pizzocaro, M., Clivati, C., Perini, F., Negusini, M., Maccaferri, G., Ricci, R., Roma, M., Bortolotti, C., Namba, K., Komuro, J., Ichikawa, R., Suzuyama, T., Watabe, K., Leute, J., Petit, G., Calonico, D., & Ido, T. (2021). A broadband VLBI system using transportable stations for geodesy and metrology: an alternative approach to the VGOS concept. *Journal of Geodesy*, *95*(4), 41. doi: 10.1007/s00190-021-01479-8

Sovers, O. J., Fanselow, J. L., & Jacobs, C. S. (1998). Astrometry and geodesy with radio interferometry: experiments, models, results. *Reviews of Modern Physics*, *70*(4), 1393-1454. doi: 10.1103/RevModPhys.70.1393

Treuhaft, R. N., & Lanyi, G. E. (1987). The effect of the dynamic wet troposphere on radio interferometric measurements. *Radio Science*, *22*(02), 251-265. doi: 10.1029/RS022i002p00251

Teke, K., Nilsson, T., Böhm, J., Hobiger, T., Steigenberger, P., García-Espada, S., ... Willis, P. (2013). Troposphere delays from space geodetic techniques, water vapor radiometers, and numerical weather models over a series of continuous VLBI campaigns. *Journal of Geodesy*, *87*(10-12), 981-1001. doi: 10.1007/s00190-013-0662-z

Thompson, A. R., Moran, J. M., & Swenson, J., George W. (2017). *Interferometry and Synthesis in Radio Astronomy, 3rd Edition.* doi: 10.1007/978-3-319-44431-4

Varenius, E., Haas, R., & Nilsson, T. (2021). Short-baseline interferometry local-tie experiments at the Onsala Space Observatory. *Journal of Geodesy*, *95*(5), 54. doi: 10.1007/s00190-021-01509-5

Xu, M. H., Anderson, J. M., Heinkelmann, R., Lunz, S., Schuh, H., & Wang, G. (2021). Observable quality assessment of broadband very long baseline interferometry system. *Journal of Geodesy*, *95*(5), 51. doi: 10.1007/s00190-021-01496-7

Xu, M. H., Anderson, J. M., Heinkelmann, R., Lunz, S., Schuh, H., & Wang, G. L. (2019). Structure Effects for 3417 Celestial Reference Frame Radio Sources. *The Astrophysical Journal Supplement Series*, *242*(1), 5. doi: 10.3847/1538-4365/ab16ea

Xu, M. H., Heinkelmann, R., Anderson, J. M., Mora-Diaz, J., Schuh, H., & Wang, G. L. (2016). The Source Structure of 0642+449 Detected from the CONT14 Observations. *The Astronomical Journal*, *152*(5), 151. doi: 10.3847/0004-6256/152/5/151

Xu, M. H., Savolainen, T., Anderson, J. M., Kareinen, N., Zubko, N., Lunz, S., & Schuh, H. (2022). Impacts of the image alignment over frequency for VLBI Global Observing System. *Astronomy and Astrophysics (in press)*. doi: https://doi.org/10.1051/0004-6361/202140840

Xu, M. H., Savolainen, T., Zubko, N., Poutanen, M., Lunz, S., Schuh, H., & Wang, G. L. (2021). Imaging VGOS Observations and Investigating Source Structure Effects. *Journal of Geophysical Research (Solid Earth)*, *126*(4), e21238. doi: 10.1029/2020JB021238

Supporting Information for "Baseline vector repeatability at the sub-millimeter level enabled by radio interferometer phase delays of intra-site baselines"

Ming H. Xu[1,2,10], Tuomas Savolainen[1,2], Sergei Bolotin[3], Simone Bernhart[4], Christian Plötz[5], Rüdiger Haas[6], Eskil Varenius[6], Guangli Wang[7], Jamie McCallum[8], Robert Heinkelmann[9], Susanne Lunz[10], Harald Schuh[10,9], Nataliya Zubko[11], and Niko Kareinen[11]

[1]Aalto University Metsähovi Radio Observatory, Metsähovintie 114,02540 Kylmälä, Finland

[2]Aalto University Department of Electronics and Nanoengineering, PL15500, FI-00076 Aalto, Finland

[3]NVI Inc. at NASA Goddard Space Flight Center, Code 61A.0, Greenbelt, MD, 20771, USA

[4]Reichert GmbH/Bundesamt für Kartographie und Geodäsie, 53121 Bonn, Germany

[5]Geodetic Observatory Wettzell, Federal Agency for Cartography and Geodesy, Sackenrieder Str. 25, 93444 Bad Kötzting, Germany

[6]Department of Space, Earth and Environment, Onsala Space Observatory, Chalmers University of Technology, 439 92 Onsala, Sweden

[7]Shanghai Astronomical Observatory, Chinese Academy of Sciences, No. 80 Nandan Raod, 200030, Shanghai, P. R. China

[8]School of Natural Sciences, University of Tasmania, Private Bag 37, Hobart TAS 7001, Australia

[9]DeutschesGeoForschungsZentrum (GFZ), Potsdam, Telegrafenberg, A17, 14473 Potsdam, Germany

[10]Institute of Geodesy and Geoinformation Science, Technische Universität Berlin, Straße des 17. Juni 135, 10623, Berlin, Germany

[11]Finnish Geospatial Research Institute, Geodeetinrinne 2, FIN-02430 Masala, Finland

Contents of this file

1. Data analysis for the baselines with only one or two global sessions
2. Table S1. List of the 24-hour sessions of baseline WETTZ13N–WETTZELL
3. Table S2. List of the Intensive sessions of baseline WETTZ13N–WETTZELL
4. Table S3. List of the 24-hour sessions of baseline NYALE13S–NYALES20
5. Table S4. List of the 24-hour sessions of baseline ISHIOKA–TSUKUB32
6. Table S5. List of the 24-hour sessions of baseline HARTRAO–HART15M
7. Table S6. Baseline vectors from the ITRF2020 that were used for the comparison of our results
8. Figure S1. Delay residuals of baseline WETTZ13N–WETTZELL from geodetic solutions of estimating a constant offset and a linear rate of the clock in session 21MAY10XA
9. Figure S2. Up residuals of antenna WETTZ13N from phase delay analysis as a function of the dZWD residuals, which are the differences of the estimated dZWDs with respect to the mean value.
10. Figure S3. Corrections for cable delays of antenna WETTZELL as a function of the temperatures in session 21MAY10XA

Introduction The detail of data analysis is presented. The VLBI sessions analyzed in the study are listed in the tables with the statistics from geodetic solutions, and three figures are shown to support the study.

1. Data analysis for the baselines with only one or two global sessions

The detail of the data analysis in Sect. 3.2 of the main body of the paper is presented here.

1.1. SESHAN13–SESHAN25

The new antenna SESHAN13 in Shanghai, China, so far participated in only one IVS session, AOV056 (February 03, 2021). The receiver cannot observe at frequencies around 2 GHz at S band, and therefore the observations of the antenna have not been used in the IVS routine data analysis. However, we analyzed the X band observations of the baseline SESHAN13–SESHAN25 to derive the baseline vector.

For this 56 m baseline, we estimated a constant parameter of dZWDs over 24 hours for antenna SESHAN13 only, and modeled the clock of antenna SESHAN13 relative to antenna SESHAN25 as a PWL function with an interval of 30 minutes to account for the rapid variations. With 411 used observations, the WRMS delay residual is 8.6 ps from the phase delay analyses and 20.9 ps from the group delay analyses. The difference between group delay analyses and phase delay analyses for this baseline is as large as 1 cm in both the east and up directions. The significant differences need to be monitored further by new observations in the future. Note that in the session both antennas do not have corrections for cable delays, which are the path delays through the cable from the frequency standard to the phasecal generator in the receiver.

This position tie allows SESHAN13 to obtain its position in the ITRF. As SESHAN13 is one of the three antennas in a Chinese domestic VGOS network aimed for the EOP determination, it can help to determine the positions of the other two antennas in the ITRF and thus a consistent set of EOP based on the observations of this domestic network.

1.2. WETTZ13S–WETTZELL

As WETTZ13S observes with a broadband and linearly polarized receiver and WETTZELL observes with a circularly polarized receiver, the mixed mode was used to make observations and perform data processing for this baseline (and other baselines between VGOS antennas and legacy antennas). The aim of the mixed mode sessions is to tie the positions of the VGOS antennas to those of the legacy antennas. In addition to the session RD1810 already reported, currently there are another two IVS mixed mode sessions available: RD2005 (June 24, 2020) and RD2006 (July 08, 2020). We should remark that the results from these mixed mode sessions may be considered as preliminary because the data processing of this new observing mode is still under investigation and may be improved in the future. The WRMS delay residual is 6.0 ps for the 370 phase delays in session RD2005 and 6.6 ps for the 423 phase delays in RD2006.

The results from both sessions have uncertainties at the sub-millimeter level in the three components. However, a significant difference of 4.3 mm was detected in the up component between the two sessions, which were observed only two weeks apart, while the differences in the horizontal plane are smaller than 0.3 mm, consistent with their formal errors. In the data processing, an important difference is that the phase calibration phases of station WETTZELL were turned on and used for session RD2005, whereas they were not used for session RD2006 through manual phase calibration (Brian Corey, personal communication, August 30, 2021).

1.3. RAEGYEB–YEBES40M

The receiver of antenna RAEGYEB is not able to observe below 3 GHz, and RD2005 is the only session that RAEGYEB participated in with the mixed mode. Therefore, without analyzing the observations at X band only, the position tie for antenna RAEGYEB, as well as for antenna SESHAN13, would have been lost. Both antennas have the cable delays measured. The measured cable delays for antenna RAEGYEB have a peak-to-peak fluctuation of more than 200 ps, which is four times that of antenna YEBES40M. Without applying the cable delays of antenna RAEGYEB, the WRMS delay residual was 17.4 ps for the 392 group delays and 9.9 ps for the 407 phase delays; it increased to 22.0 ps for the same set of group delays and 15.5 ps for the 417 used phase delays when the cable delays were applied. The cable delays introduced non-negligible additional noise of about 12 ps, a demonstration that there are unknown issues with the cable delay corrections.

The results are based on the solutions without applying the cable delay corrections of antenna RAEGYEB. The difference in the baseline vector estimates between group delays and phase delays is not significant with respect to the uncertainties of the group delay result. Applying the cable delay corrections would change the Up position of antenna RAEGYEB by 5.3 mm for group delay analyses and by 6.3 mm for phase delay analyses.

1.4. KOKEE12M–KOKEE

With 422 available observations of baseline KOKEE12M–KOKEE in session RD2006, the WRMS delay residual is 15.7 ps for the 382 group delays and 3.7 ps for the 385 phase delays. Note that antenna KOKEE has the cable delays directly measured, and antenna KOKEE12M has the proxy cable delay corrections through an indirect way. The results of this baseline from session RD2005 are not reported because the WRMS delay residuals are significantly larger for both phase and group delays than those from session RD2006 due to yet unknown reasons.

1.5. `ONSALA60–ONSA13NE–ONSA13SW`

We report the results of these baselines based on the phase delays in sessions RD2005 and RD2006. As antenna `ONSA13NE` cannot observe at 2.0 GHz, its observations in session RD2005 were removed in the IVS routine data analysis, and its observations in session RD2006 were even not processed by the IVS at the visibility level. Nevertheless, we analyzed its observations in session RD2005.

Both the dZWDs and the clocks were estimated for antennas `ONSA13NE` and `ONSA13SW` as PWL functions with an interval of one hour (`ONSALA60` was the reference). The WRMS delay residual is 3.0 ps for the 998 phase delays of the three baselines in session RD2005, and it is 5.3 ps for the 400 phase delays of baseline `ONSALA60–ONSA13SW` in session RD2006. Note that there is a difference of 3.24 mm in the up direction of baseline `ONSALA60–ONSA13SW` between these two sessions, while the differences in the horizontal directions are less than half a millimeter, insignificant to the uncertainties.

Table S1: List of the 24-hour sessions of baseline `WETTZ13N–WETTZELL` with usable observations as of July 2021. The number of the used observables n_{used} and the WRMS delay residual r_{WRMS} are presented for both types of observables.

Session	n_{total}	Group delays			Phase delays		
		n_{used}	r_{WRMS} [ps]	σ_{add} [ps]	n_{used}	r_{WRMS} [ps]	σ_{add} [ps]
19JAN29XH	293	277	31.6	33.3	277	4.1	4.3
19MAR26XH	360	300	41.1	42.8	295	4.4	4.6
19APR11XE	246	200	19.6	21.1	199	4.4	4.7
19APR15XA	188	185	7.3	7.9	186	3.6	3.9
19APR23XA	97	97	7.8	9.1	95	2.4	2.8
19APR25XE	162	144	12.6	14.0	145	3.0	3.3
19MAY02XE	160	145	14.7	16.3	148	4.1	4.6

Continued on next page

Table S1 – continued from previous page

Session	n_{total}	Group delays			Phase delays		
		n_{used}	r_{WRMS} [ps]	σ_{add} [ps]	n_{used}	r_{WRMS} [ps]	σ_{add} [ps]
19MAY07XA	77	76	6.3	7.8	77	3.1	3.8
19OCT08XA	298	267	9.0	9.5	279	2.8	2.9
19OCT10XE	308	259	9.8	10.2	276	2.7	2.8
19OCT17XE	384	377	14.4	15.0	377	2.8	2.9
19OCT21XA	106	100	6.5	7.6	104	1.8	2.1
19OCT24XE	381	370	11.2	11.7	373	2.9	3.0
19OCT28XA	244	233	13.9	14.8	241	2.9	3.1
19OCT30XE	352	341	15.9	16.6	343	3.0	3.1
19NOV04XA	85	84	7.4	9.0	85	3.0	3.7
19NOV07XE	380	362	16.1	16.8	370	2.7	2.8
19NOV18XA	138	136	10.4	11.6	135	2.6	2.9
19NOV19XH	371	364	40.4	42.1	354	2.8	2.9
19NOV21XE	290	255	10.8	11.4	260	2.9	3.1
19NOV26XE	302	275	16.9	17.8	274	3.3	3.5
19DEC05XE	366	324	17.2	18.5	324	3.3	3.6
19DEC10XH	404	387	53.7	55.9	384	3.9	4.1
19DEC12XE	293	252	22.8	24.0	256	4.0	4.2
19DEC17XA	158	146	6.1	6.8	148	2.9	3.2
19DEC19XE	329	308	13.5	14.2	309	2.6	2.7
20JAN02XE	429	396	17.8	18.4	399	2.9	3.1
20JAN09XE	338	310	17.5	18.2	307	2.7	2.8
20JAN16XE	303	267	15.9	16.7	266	3.1	3.3
20JAN23XE	356	337	15.6	16.2	340	2.8	3.0
20JAN27XA	172	171	12.1	13.2	170	2.7	3.0
20JAN30XE	349	327	17.3	18.0	325	3.3	3.4
20FEB06XE	353	306	19.7	20.5	306	3.0	3.2
20FEB10XA	170	146	12.4	13.8	147	3.3	3.7
20FEB13XE	247	174	19.0	20.7	174	5.3	5.8
20FEB17XA	159	159	11.3	12.4	157	3.4	3.7
20FEB24XA	229	226	10.8	11.5	225	2.8	3.0
20MAR02XA	141	137	11.3	12.7	139	2.3	2.6
20MAR05XE	451	372	16.3	17.0	375	3.8	4.0
20MAR09XA	176	175	19.2	20.9	172	2.6	2.8
20MAR19XE	306	266	17.9	18.8	263	3.0	3.2
20MAR26XE	306	258	15.8	16.6	255	2.4	2.5
20APR02XE	286	187	16.5	17.6	186	2.8	3.0
20APR08XE	275	252	17.2	18.1	247	2.5	2.7
20APR16XE	299	261	16.2	17.1	261	2.8	2.9
20APR22XE	339	315	17.0	17.7	314	3.3	3.4
20APR27XA	146	140	14.4	16.0	141	3.5	3.9
20APR29XE	302	239	16.1	17.1	241	3.2	3.4
20MAY11XA	61	61	9.9	13.2	61	3.1	4.2

Continued on next page

Table S1 – continued from previous page

Session	n_{total}	Group delays			Phase delays		
		n_{used}	r_{WRMS} [ps]	σ_{add} [ps]	n_{used}	r_{WRMS} [ps]	σ_{add} [ps]
20MAY26XA	138	133	9.5	10.7	132	3.3	3.7
20JUN08XA	124	124	6.2	7.0	123	2.9	3.3
20JUN18XE	309	273	13.7	14.4	272	3.2	3.4
20JUN25XE	310	252	13.9	14.6	253	2.8	2.9
20JUL01XE	252	225	19.2	20.4	224	3.5	3.7
20JUL09XE	295	266	15.1	15.9	259	2.6	2.7
20JUL23XE	297	272	15.9	16.7	270	4.2	4.4
20JUL30XE	270	238	14.0	14.9	235	5.1	5.4
20AUG06XE	265	153	13.9	15.3	200	6.3	6.8
20AUG13XE	359	308	13.1	13.8	311	5.2	5.4
20AUG20XE	209	152	12.0	13.0	152	3.6	4.0
20AUG27XE	332	297	11.5	12.1	295	4.0	4.2
20SEP03XE	335	286	13.6	14.3	282	3.2	3.4
20SEP10XE	353	320	11.9	12.9	323	3.6	3.9
20SEP17XE	236	212	17.9	19.0	214	4.5	4.8
20SEP24XE	266	190	17.0	19.3	190	3.3	3.8
20NOV12XE	227	166	13.4	14.6	169	4.3	4.7
20NOV26XE	261	223	16.3	17.3	226	5.1	5.4
20DEC10XE	335	301	16.9	17.8	303	5.4	5.7
20DEC22XE	327	289	19.1	20.1	288	4.8	5.1
21JAN04XA	310	300	14.8	15.6	303	5.3	5.6
21JAN07XE	324	227	22.9	24.4	231	6.1	6.5
21JAN21XE	327	251	19.4	20.4	252	4.8	5.1
21JAN25XA	240	218	12.5	13.2	221	6.5	6.8
21FEB01XA	386	376	17.6	18.3	381	8.1	8.4
21FEB08XA	424	418	17.4	17.9	418	5.2	5.3
21FEB16XA	411	407	14.4	14.8	409	5.4	5.6
21FEB18XE	270	224	15.9	16.9	227	7.1	7.6
21FEB22XA	414	411	17.0	17.5	412	4.8	4.9
21MAR04XE	378	322	16.1	16.8	324	4.5	4.7
21MAR08XA	317	307	14.6	15.4	313	4.6	4.8
21MAR15XA	284	274	10.8	11.4	277	4.3	4.5
21MAR18XE	345	277	17.7	18.6	280	4.7	4.9
21MAR23XA	402	394	13.1	13.6	397	5.2	5.4
21MAR25XE	261	237	16.1	17.1	238	4.7	5.0
21MAR31XE	354	288	13.6	14.3	297	4.6	4.8
21APR19XA	436	423	11.7	12.1	428	4.8	4.9
21APR22XE	284	274	17.3	18.2	274	4.2	4.4
21APR29XE	264	239	18.7	19.9	243	3.9	4.1
21MAY03XA	356	354	15.1	15.7	355	4.7	4.9
21MAY06XE	279	250	15.8	16.8	254	5.5	5.9
21MAY10XA	434	431	9.7	10.0	431	3.7	3.8

Continued on next page

Table S1 – continued from previous page

Session	n_{total}	Group delays			Phase delays		
		n_{used}	r_{WRMS} [ps]	σ_{add} [ps]	n_{used}	r_{WRMS} [ps]	σ_{add} [ps]
21MAY13XE	287	264	14.5	15.3	271	4.7	4.9
21JUN09XE	525	499	13.3	13.7	495	4.4	4.5
22JAN31XA	347	325	14.2	14.8	328	5.1	5.3
22FEB03XE	345	322	16.3	17.0	323	4.1	4.3
22FEB07XA	375	364	11.6	12.1	364	3.8	4.0
22FEB10XE	384	375	12.9	13.4	373	3.8	4.0
22FEB21XA	359	348	16.4	17.1	348	4.4	4.6
22FEB24XE	473	461	14.8	15.3	461	4.3	4.4
22FEB28XA	532	518	19.7	20.3	516	4.6	4.7
22MAR10XE	458	449	22.1	22.8	453	5.0	5.2
22MAR24XE	467	463	18.9	19.5	463	6.4	6.6
22MAR31XE	387	381	22.4	23.3	381	4.7	4.9
22APR07XE	410	403	13.4	13.8	400	4.2	4.3
22MAY05XE	357	347	11.1	11.6	346	3.4	3.5
22JUN09XE	321	301	13.4	14.0	297	3.8	4.0
22JUN16XE	357	345	18.2	19.0	339	3.9	4.1

Table S2: Intensive session list of baseline WETTZ13N–WETTZELL as of July 2021. The number of the used observables n_{used}, the WRMS delay residual r_{WRMS}, and the additive sigma σ_{add} to achieve the reduced χ^2 being unity are presented for both types of observables.

Session	n_{total}	Group delays			Phase delays		
		n_{used}	r_{WRMS} [ps]	σ_{add} [ps]	n_{used}	r_{WRMS} [ps]	σ_{add} [ps]
19MAR04XK	43	39	12.1	13.2	43	2.3	2.5
19MAR18XK	45	43	11.4	12.3	43	3.3	3.5
19MAR25XK	46	46	7.1	7.6	46	5.3	5.7
19APR15XK	39	37	7.8	8.5	37	2.8	3.0
19APR29XK	48	46	9.5	10.2	47	2.8	3.0
19MAY06XK	46	43	7.1	7.6	42	1.7	1.8
19OCT14XK	40	37	5.0	5.4	39	2.3	2.5
19OCT21XK	50	49	5.9	6.3	49	1.8	1.9
19OCT28XK	50	50	9.0	9.6	50	4.5	4.8
19NOV04XK	49	48	12.2	13.0	47	2.0	2.2
19NOV11XK	49	47	10.1	10.9	47	2.0	2.2
19NOV18XK	51	51	9.3	9.9	51	2.5	2.7
20MAR02XK	47	45	15.9	17.1	45	2.5	2.7
20MAR09XK	47	47	12.4	13.3	47	2.6	2.8
20MAR16XK	38	35	10.7	11.8	35	1.7	1.9
20MAR23XK	37	35	9.8	10.8	36	2.3	2.5
20MAR30XK	48	42	8.3	8.9	46	3.7	4.0
20APR20XK	37	34	8.1	8.9	34	2.0	2.2
20APR27XK	40	35	8.0	8.8	37	2.4	2.6
20MAY04XK	37	32	9.3	10.3	33	2.2	2.4
20MAY11XK	47	46	10.1	10.9	46	2.0	2.2
20MAY18XK	41	41	8.8	9.6	40	2.3	2.5
20MAY25XK	47	43	10.9	11.7	43	3.4	3.7
20JUN08XK	47	45	9.6	10.3	45	3.3	3.5
20JUN15XK	48	44	8.2	9.1	44	2.3	2.5
20JUN22XK	39	33	7.3	8.1	33	2.0	2.2
20JUN29XK	38	28	6.7	7.5	29	3.2	3.6
20JUL06XK	39	35	12.9	14.2	35	3.5	3.8
20JUL13XK	41	37	5.5	6.0	38	2.0	2.2
20JUL20XK	40	38	9.2	10.0	38	2.8	3.0
20JUL27XK	40	38	10.6	11.5	39	3.4	3.7
20AUG03XK	38	33	11.4	12.7	34	4.0	4.4
20AUG24XK	38	33	8.8	9.8	35	6.8	7.5
20AUG31XK	40	31	7.7	8.6	32	3.0	3.3
20SEP07XK	43	35	7.9	8.7	37	3.3	3.6
20SEP14XK	43	37	6.6	7.2	38	2.3	2.5
20SEP21XK	42	38	5.1	5.5	39	4.0	4.3

Continued on next page

Table S2 – continued from previous page

Session	n_{total}	Group delays			Phase delays		
		n_{used}	r_{WRMS} [ps]	σ_{add} [ps]	n_{used}	r_{WRMS} [ps]	σ_{add} [ps]
20SEP28XK	41	38	8.8	9.6	39	3.1	3.4
20OCT12XK	38	35	11.5	12.6	35	5.0	5.5
20NOV09XK	40	37	7.0	7.6	40	3.4	3.7
21JAN11XK	45	28	14.3	16.1	31	5.0	5.6
21JAN18XK	43	32	11.0	12.2	33	4.3	4.8
21FEB01XK	44	44	12.1	13.0	44	3.1	3.3
21FEB08XK	41	40	14.4	15.7	40	3.0	3.3
21MAR01XK	43	40	7.3	7.9	41	4.4	4.8
21MAR08XK	42	37	8.4	9.1	38	2.2	2.4
21MAR15XK	44	42	8.6	8.7	43	4.8	5.2
21MAR22XK	44	34	13.1	14.4	36	4.6	5.1
21MAR29XK	43	42	4.6	4.9	40	1.9	2.1
21APR12XK	42	35	22.6	24.8	35	3.5	3.8
21APR26XK	42	36	12.4	13.6	37	3.8	4.1
21MAY03XK	35	34	6.2	6.8	34	4.1	4.5
21MAY10XK	41	35	6.2	6.8	36	1.9	2.1
21MAY17XK	54	53	16.0	17.0	53	3.8	4.0
21MAY31XK	39	38	9.6	10.4	38	3.9	4.2
21JUN07XK	38	34	5.8	6.4	34	2.8	3.1
21JUN21XK	41	37	9.1	9.9	37	2.5	2.7
21JUN28XK	40	35	8.4	9.2	34	3.2	3.5

Table S3: Session list of baseline NYALE13S–NYALES20. The number of used observables n_{used} and the WRMS delay residual r_{WRMS} is presented for both group delays and phase delays (at X band). For comparison, these two statistics from the official IVS results based on the observables at S/X band are presented in the last two columns.

Session	n_{total}	Group delays			Phase delays			S/X-band delays[1]		
		n_{used}	r_{WRMS} [ps]	σ_{add} [ps]	n_{used}	r_{WRMS} [ps]	σ_{add} [ps]	n_{used}	r_{WRMS} [ps]	σ_{add} [ps]
20MAY26XA	155	152	25.3	22.3	151	17.2	19.4	76	49.1	43.1
20JUN22XA	305	297	24.7	20.8	298	17.3	18.9	291	30.4	25.2
21MAY25XA	286	207	58.1	49.1	213	17.2	19.3	185	65.6	53.1
21MAY31XA	363	313	48.7	38.5	317	15.8	17.1	306	54.0	42.1
21JUN07XA	300	295	18.6	17.1	295	13.9	15.2	277	25.4	22.5
21JUN09XE	341	333	26.2	22.3	334	16.5	17.8	243	35.4	–
21JUN14XA	299	216	40.4	29.3	220	16.5	18.3	188	57.6	48.3
21JUN17XE	484	475	32.8	25.3	477	19.5	19.9	381	71.1	–
21JUN21XA	114	107	27.4	22.5	106	12.6	16.1	102	40.0	–
21JUN24XE	329	307	46.6	36.5	307	15.2	16.5	252	86.0	72.7
22FEB07XA	263	260	30.3	32.9	232	15.4	17.3	251	40.4	30.0
22FEB24XE	361	342	43.3	46.6	309	15.3	17.2	145	87.2	70.6
22MAR22XA	328	326	32.2	34.6	296	16.5	18.1	318	44.2	32.3
22MAR24XE	378	372	35.7	38.4	346	15.7	17.4	107	76.6	62.6
22APR25XA	394	394	31.4	33.4	390	17.2	18.5	392	42.2	30.9
22MAY12XE	359	355	33.2	36.1	282	13.0	14.9	104	41.3	49.7
22MAY23XA	339	337	26.3	28.3	330	11.9	12.9	333	36.8	27.8
22JUN09XE	251	236	52.8	58.0	234	15.2	17.7	173	71.2	53.0
22JUN16XE	263	259	30.7	33.7	261	16.8	18.7	62	55.6	41.8

Table S4. Session list of baseline ISHIOKA–TSUKUB32. The number of used observables and the WRMS delay residual are presented for both types of observables.

Session	n_{total}	Group delays		Phase delays	
		n_{used}	r_{WRMS} [ps]	n_{used}	r_{WRMS} [ps]
15AUG26XA	238	220	14.00	219	10.40
15OCT19XA	396	365	16.00	355	13.20
15NOV10XH	175	172	17.10	167	9.60
15NOV12XF	448	420	20.90	399	12.90
15NOV16XA	393	357	21.60	335	13.40
15DEC07XA	347	337	16.50	327	12.40
15DEC14XA	312	296	18.80	286	13.90
15DEC15XH	169	169	22.60	168	14.50
15DEC16XA	288	236	23.20	238	11.80
16APR11XA	447	432	16.30	420	13.50
16MAY17XA	361	342	21.10	331	14.00
16JUN13XA	454	427	23.10	405	15.60
16OCT24XA	448	426	25.30	413	16.50
16OCT31XA	463	437	19.30	403	14.60
16DEC05XA	195	180	17.70	178	13.60
16DEC20XA	361	341	9.90	341	9.00
16DEC27XA	352	338	14.90	314	11.00

Table S5. Session list of baseline HARTRAO–HART15M. The number of used observables and the WRMS delay residual are presented for both types of observables.

Session	n_{total}	Group delays			Phase delays		
		n_{used}	r_{WRMS} [ps]	σ_{add} [ps]	n_{used}	r_{WRMS} [ps]	σ_{add} [ps]
13AUG05XA	117	89	5.7	6.4	94	4.9	5.8
13AUG26XA	109	109	12.2	13.8	109	9.7	11.3
13SEP09XA	262	256	11.9	9.5	257	8.6	9.1
13NOV25XA	92	92	9.8	10.6	92	8.8	9.8
14AUG04XA	218	212	12.6	12.1	212	10.1	10.9
15JUL27XA	235	233	12.9	11.3	233	10.3	10.8
15NOV09XA	248	243	13.2	12.4	243	10.0	10.5
17OCT02XA	158	158	9.1	9.2	154	7.6	8.4

Table S6. Baseline vectors from the ITRF2020(see `https://itrf.ign.fr/en/solutions/ITRF2020` for more details) (units: mm).

Baseline	Monument	X	σ_X	Y	σ_Y	Z	σ_Z	L	σ_L
Wn–Wz	7387–7224	−88036.50	1.28	−38731.90	1.20	77162.90	1.50	123307.33	1.36
Ns–Ny	7392–7331	1391823.40	25.21	605216.00	25.31	−256263.50	27.42	1539197.77	25.29
Hh–Ht	7232–7378	48035.80	1.98	−102302.80	1.63	4129.10	1.84	113094.43	1.70
Ws–Wz	7388–7224	−119343.30	1.61	−89238.20	1.44	113294.80	1.84	187195.06	1.66
Yj–Ys	7389–7386	−69318.70	2.30	145344.80	1.50	108530.90	2.30	194188.44	1.89
K2–Kk	7623–7298	−6075.90	3.89	19218.50	2.97	23722.70	3.45	31129.31	3.29
On–Ow	7213–7637	340934.30	2.94	−383169.50	1.97	−169945.90	4.51	540311.64	2.72
Oe–On	7636–7213	−283455.50	2.47	346477.20	1.79	138820.20	3.54	468683.82	2.25
Oe–Ow	7636–7637	57478.80	3.62	−36692.30	2.41	−31125.70	5.56	74959.63	3.80

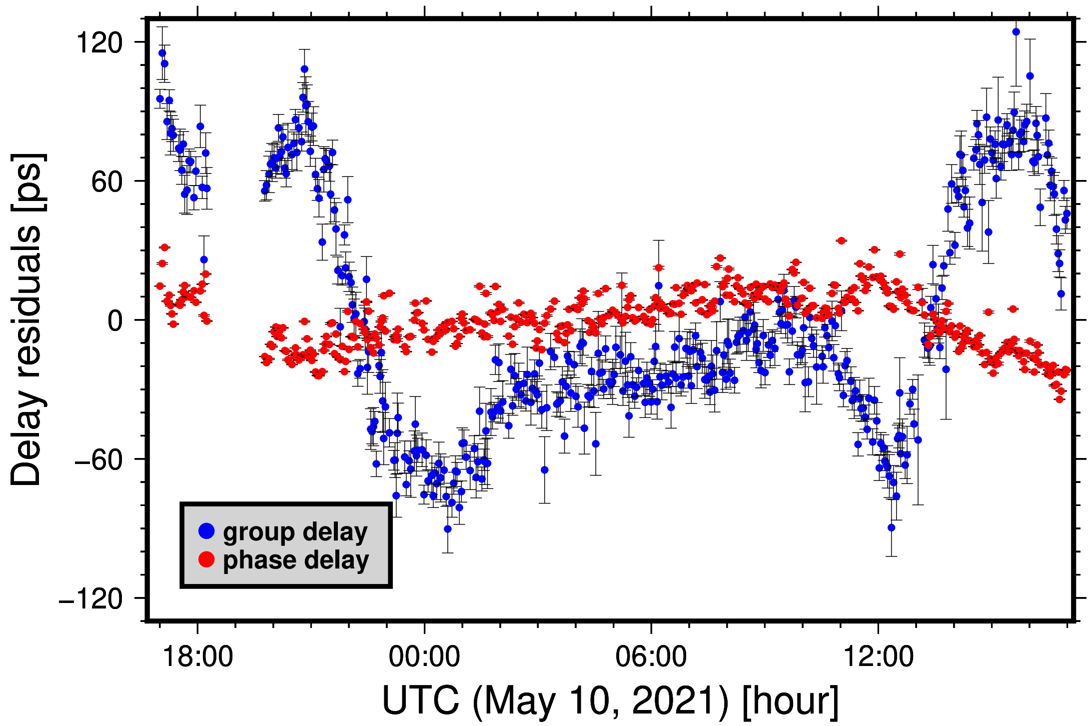

Figure S1. Delay residuals of baseline `WETTZ13N–WETTZELL` from geodetic solutions when estimating a constant offset and a linear rate of the clock (two parameters only) based on group delays (blue dots) and phase delays (red dots) in session 21MAY10XA. For the direction comparison of the group delays and the phase delays, refer to Fig. 2 in the main body of the paper.

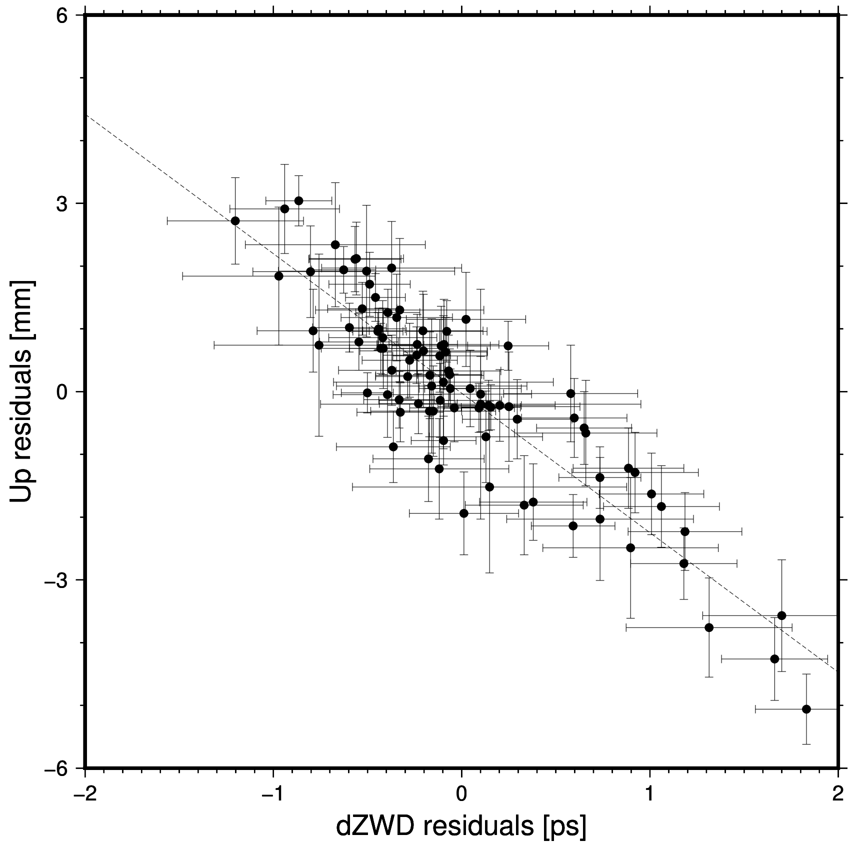

Figure S2. Up residuals of baseline vector `WETTZ13N–WETTZELL` from phase delay analysis as a function of the dZWD residuals, which are the differences of the estimated dZWDs with respect to the mean value.

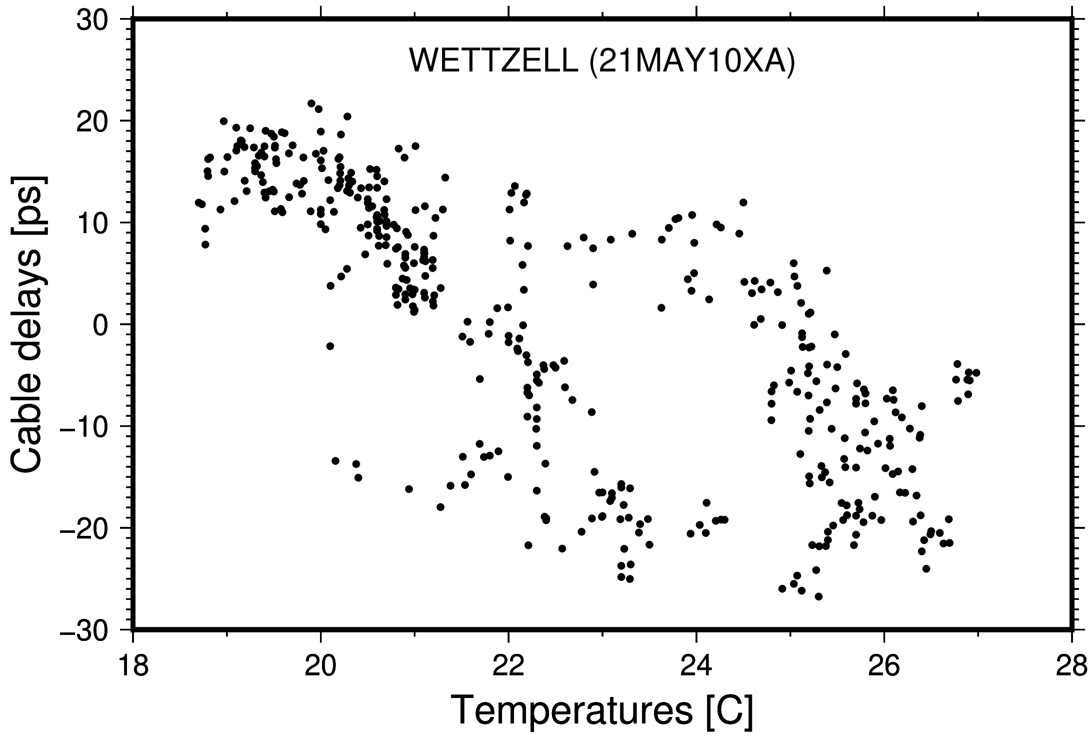

Figure S3. Corrections for cable delays of antenna `WETTZELL` in session 21MAY10XA as a function of the temperatures at the site.